International Journal of Heat and Mass Transfer 149 (2020) 119211

Contents lists available at ScienceDirect

International Journal of Heat and Mass Transfer

journal homepage: www.elsevier.com/locate/hmt

An artificial neural network model to predict mini/micro-channels saturated flow boiling heat transfer coefficient based on universal consolidated data

Yue Qiu[a,#], Deepak Garg[b,#], Liwei Zhou[a], Chirag R. Kharangate[a,*], Sung-Min Kim[c], Issam Mudawar[d]

[a] Department of Mechanical and Aerospace Engineering, Case Western Reserve University, 10900 Euclid Avenue, Cleveland OH 44106, USA
[b] Mechanical and Aerospace Engineering Department, University of California, Los Angeles CA 90095, USA
[c] School of Mechanical Engineering, Sungkyunkwan University, 300 Cheoncheon-dong, Suwon 16419, Republic of Korea.
[d] School of Mechanical Engineering, 585 Purdue Mall, West Lafayette IN 47907-2088, USA

ARTICLE INFO

Article history:
Received 26 September 2019
Revised 8 December 2019
Accepted 9 December 2019
Available online 23 December 2019

Keywords:
ANN
Universal data
Saturated
Flow boiling
Heat transfer

ABSTRACT

Flow boiling in mini/micro channels is a very effective technique for meeting the high dissipating requirements of thermal management systems. However, accurate prediction of heat transfer coefficients remains an elusive task because of the complex fluid and thermal behavior in these two-phase systems. In this study, a machine learning based approach for predictingheat transfer for saturated flow boiling in mini/micro channels is proposed. A consolidated database of 16953 data points for flow boiling heat transfer in mini/micro-channels is amassed from 50 sources that includes 16 working fluids, reduced pressures of 0.0046 – 0.77, hydraulic diameters of 0.15mm – 6.5mm, mass velocities of $19 < G < 1608 kg/m^2s$, liquid-only Reynolds numbers of 27 – 55270 and flow qualities of 0 – 1. An Artificial Neural Network (ANN) model is developed based on the universal consolidated database that was split into training data and test data, and used to predict the saturated flow boiling heat transfer coefficients. An optimization is conducted and ANN model architecture is selected which consists of dimensionless input parameters: *Bd, Bo, Co,* Fr_g, Fr_{go}, Fr_f, Fr_{fo}, Pr_g, Pr_f, Re_g, Re_{go}, Re_f, Re_{fo}, Su_g, Su_f, We_g, We_{go}, We_f, and We_{fo}, and hidden layers (75,70,60,50,30,20,10) that predicts the test data with an *MAE* of 14.3%. The ANN model is superior to universal correlations for saturated flow boiling heat transfer at predicting the test data, even predicting individual databases with high accuracy. The robustness of the ANN model was tested by excluding databases from the training datasets altogether and utilized to predict these excluded databases. The ANN model did extremely well when a working fluid data was included in the training dataset, and poorly when a working fluid data was excluded from training dataset. The use of a universal ANN model utilizing a consolidated database can become an extremely useful tool when it comes to predicting heat transfer coefficients for saturated flow boiling in mini/micro channels.

1. Introduction

1.1. Flow boiling in mini/micro-channel

The past few decades have seen a significant increase in the amount of heat dissipation requirements in systems and devices across many applications, including high performance computers, electrical vehicle power electronics, avionics, directed energy laser, and microwave weapon systems [1]. This change has not only happened due to technological advances making systems and devices smaller, but also due to a need to continuously improve their power densities, which can be achieved with smaller, higher-capacity thermal management designs. Flow boiling in small channels, designated as "mini/micro channels", has been recognized as a very effective technique in meeting the high dissipating requirements [2]. This is because they provide many advantages in comparison to traditional cooling schemes: (1) High surface to volume ratios lead to increased power densities in comparison to traditional systems. (2) Utilizing boiling leads to orders of magnitude enhancement in heat transfer coefficient because the system relies on latent heat in addition to sensible heating to achieve the heat dissipation. (3) The flow rates requirements are significantly lower

* Corresponding author.
E-mail address: chirag.kharangate@case.edu (C.R. Kharangate).
# Contributed equally to this paper.

https://doi.org/10.1016/j.ijheatmasstransfer.2019.119211
0017-9310/

Nomenclature

Bd	bond number, $Bd = g(\rho_f - \rho_g)D_h^2/\sigma$
Bo	boiling number, $Bo = q''_H/Gh_{fg}$
C	confinement number
Co	convection number, $Co = [(1-x)/x]^{0.8}(\rho_g/\rho_f)^{0.5}$
c_p	specific heat at constant pressure
c_v	specific heat at constant volume
D_h	hydraulic diameter of flow channel
E	total error
F	enhancement factor
E_m	loss function
Fr_f	saturated liquid Froude number, $Fr_f = [G(1-x)]^2/(\rho_f^2 gD_h)$
Fr_g	saturated vapor Froude number, $Fr_g = (Gx)^2/(\rho_g^2 gD_h)$
Fr_{fo}	liquid-only Froude number, $Fr_{fo} = G^2/(\rho_f^2 gD_h)$
Fr_{go}	vapor-only Froude number, $Fr_{go} = G^2/(\rho_g^2 gD_h)$
F_f	fluid-dependent parameter
f	activation function
G	mass velocity
g	gravity acceleration
h	heat transfer coefficient
$h_{tp,exp}$	experiment measured two-phase heat transfer coefficient
$h_{tp,pred}$	predicted two-phase heat transfer coefficient
h_{fg}	latent heat of vaporization
i	connecting node i
j	connecting node j
k	liquid conductivity
L	total number of input and output layers
l	layer
m	training example
M	number of training examples; molecular mass
MAE	mean absolute error
MSE	mean square error
n	number of input parameters
P	pressure
P_c	critical pressure
Pe_f	saturated liquid Peclet number, $Pe_f = Re_f\ Pr_f$
Pe_g	saturated vapor Peclet number, $Pe_g = Re_g\ Pr_g$
P_F	wetted perimeter of channel
P_H	heated perimeter of channel
P_R	reduced pressure, $P_R = P_c/P$
Pr_f	saturated liquid Prandtl number, $Pr_f = \mu_f c_{pf}/k_f$
Pr_g	saturated vapor Prandtl number, $Pr_g = \mu_g c_{pg}/k_g$
q''	heat flux
q''_H	heat flux based on heated perimeter of channel
R	relative roughness, $R = e/D_h$; Pearson's correlation coefficient
R^2	coefficient of determination
Re_f	saturated liquid Reynolds number, $Re_f = G(1\text{-}x)D_h/\mu_f$
Re_g	saturated vapor Reynolds number, $Re_g = GxD_h/\mu g$
Re_{fo}	liquid-only Reynolds number, $Re_{fo} = GD_h/\mu_f$
Re_{go}	vapor-only Reynolds number, $Re_{go} = GD_h/\mu g$
S	output, suppression factor
Su_f	saturated liquid Suratman number,
Su_g	saturated vapor Suratman number,
t	target value of training example
T	temperature
w	weight of connecting node
We_f	saturated liquid Weber number, $We_f = [G(1-x)]^2 D_h/(\rho_f\sigma)$
We_g	saturated vapor Weber number, $We_g = (Gx)^2 D_h/(\rho_g\sigma)$
We_{fo}	liquid-only Weber number, $We_{fo} = G^2 D_h/(\rho_f\sigma)$
We_{go}	vapor-only Weber number, $We_{go} = G^2 D_h/(\rho_g\sigma)$
Xtt	Lockhart-Martinelli parameter, $Xtt = (\mu_f/\mu_g)^{0.1}[(1-x)/x]^{0.9}(\rho_g/\rho_f)^{0.5}$
x	quality, value of the node

Greek Symbols

α	vapor void fraction
α_r	regularization parameter
β	aspect ratio, exponential decay rate
δ	error at the node
ε	percentage data predicted within ±50%,
θ	percentage data predicted within ±30%,
μ	dynamic viscosity
λ	learning rate
ρ	density
σ	surface tension

Subscripts

c	critical
cb	convective boiling
exp	experimental
f	saturated liquid, fluid
fo	liquid only
g	saturated vapor
go	vapor only
l	liquid
nb	nucleate boiling
$pred$	predicted
tp	two phase
w	heated wall; inner wall

in comparison to single-phase liquid flows leading to smaller liquid inventories. (4) There is more axial temperature uniformity because during boiling as the coolant temperature stays close to its saturation temperatures. (5) Advances in manufacturing has led to relative ease of fabrication of microchannel geometries across different materials.

Typical circular and rectangular microchannel configurations for single-channel and multi-channel designs are shown in Fig. 1. Flow boiling heat transfer in mini/micro channels depends strongly on the flow pattern and the corresponding thermal behavior in these channels. Dominant flow patterns, which are observed in mini/micro-channels, include bubbly, slug, annular and mist flow. However, the axial span of each of these patterns is dependent on the dominant flow regime, and two common flow regimes have been identified, nucleate boiling dominant and convective boiling dominant as shown in Fig. 2 [3]. The specific regime observed in mini/micro channels is dependent on the channel dimensions and operating conditions. In nucleate boiling dominant regime, the flow is dominated by bubbly and slug flow with a small section of annular flow before reaching dryout. In this regime, the heat transfer coefficient increases fast initially in the bubble region before gradually decreasing with increase in flow quality due to a continuous suppression of nucleate boiling. Before dryout, there is a sharp reduction in heat transfer coefficient, which is followed by a slow increase in the mist flow regime. In convective boiling dominant regime, the flow is dominated by annular flow with a small section of bubbly and slug flow. In this regime, the heat transfer coefficient gradually increases with increase in flow quality due to initiation of bubble flow, followed by a gradual reduction in annular film thickness along the channel. Even in this regime, before dryout, there is a sharp reduction in heat transfer coefficient,

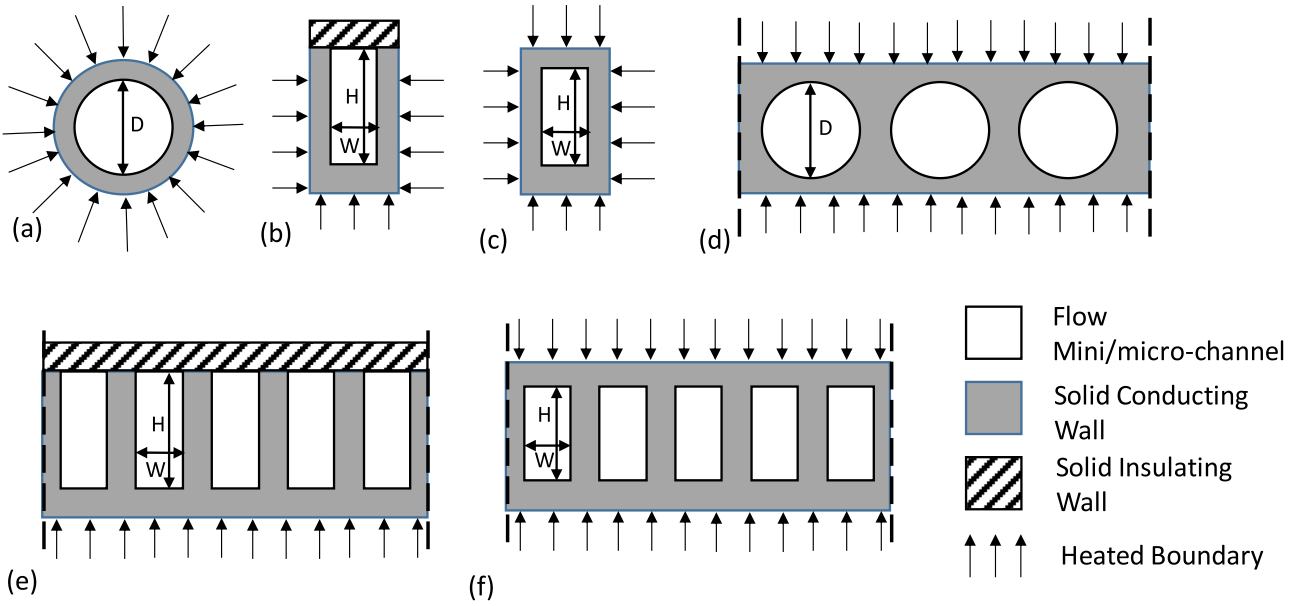

Fig. 1. Cross-sections of typical mini/micro-channel configurations: (a) circular single channel, (b) rectangular single channel 3-sided heating, (c) rectangular single channel uniform heating, (d) circular multiple channel, (e) rectangular multiple channel 3-sided heating, and (f) rectangular multiple channel uniform heating

which is followed by a slow increase in mist flow regime. Considering the complex behavior, it is not easy to accurately predict flow boiling heat transfer coefficients in mini/micro channels.

1.2. Predicting heat transfer coefficient

The most common and widely used approach to predicting heat transfer coefficient in saturated flow boiling is the use of empirical and semi-empirical correlations [4,5]. These correlations are based on experiments conducted by researchers on a few fluids tested over a range of geometric and flow parameters. Due to the complex physics behind boiling flows, they should not be used to predict outside the tested range because that can lead to wrong design decisions. Another predicting method to predict the heat transfer coefficients tries to capture the underlying fluid flow and thermal transport physics utilizes a control volume-based modeling strategy. This includes both theoretical models [6] and computational fluid dynamics (CFD) simulations [7]. Recent progress in high-performance computing facilitates the employment of the highly accurate Direct Numerical Simulation, that enables direct solution of the Navier–Stokes equations [8]. However, this technique requires extremely high computational resources.

An effective predicting approach which is very useful involves the use of “universal” correlations that are based on a large database of experiments conducted by researchers worldwide including numerous fluids and an extensive range of geometric and flow parameters [3,9–13]. A good universal correlation developed for saturated flow boiling in small channels is the study by Bertsch et al. [12]. They amassed data from 14 sources, and the correlation provided reasonably good predictions against the entire database, evidenced by an overall *MAE* of 28.0%. Another good example for universal correlation is the study by Kim and Mudawar [3], who developed a generalized correlation for the pre-dryout two-phase heat transfer coefficient associated with saturated flow boiling in mini/micro-channels. They amassed data from 37 sources, and its accuracy was validated for various working fluids and over very broad ranges of operating conditions. This correlation provided good predictions against the entire pre-dryout database, evidenced by an overall *MAE* of 20.3%. Also, in a recent study, Fang et al. [13] developed a universal correlation for the two-phase heat transfer coefficient associated with saturated flow boiling in mini/micro-channels. They amassed data from 101 sources, and its accuracy was validated for various working fluids and over very broad ranges of operating conditions. This correlation utilized a fluid-dependent parameter that requires an experimental fit based on the specific working fluid. This correlation provided very good predictions against the entire database, evidenced by an overall *MAE* of 4.5%.

1.3. Artificial neural network in thermal analysis

Conducting two-phase experiments or full CFD simulations require a high cost and time commitment. Parameters like heat transfer coefficients in two-phase flows are usually a function of many independent dimensionless groups, each of them valid over a finite range of values. The relationship between these parameters and their relevance to heat transfer coefficients can be deduced using new computing techniques. A promising technique which can be applied to correlating heat transfer coefficients is the use of soft-computing. In the past three decades, we have seen unprecedented development of soft computing techniques, such as Artificial Neural Networks (ANNs), Genetic Algorithm (GA), Genetic Programming (GP), Fuzzy-logic Control, and Data Mining, and its application to many scientific and engineering practices. Out of these, ANNs, which are inspired by biological nervous systems of humans, learn to perform tasks by utilizing available data, without the need for programmed task-specific rules. ANNs see a lot of applications in pattern recognition, system identification, and dynamic control, to name a few. In the last two decades, they have also been successfully implemented for analyzing many thermal systems [14–21]. Some early work in modeling and correlating heat transfer data with ANNs was performed by Thibault et al. [22]. Jambunathan et al. [23] applied the ANNs to model one-dimensional transient heat conducting for liquid crystal thermography and predict the convective heat transfer coefficients inside a duct. Mazzola [24] used an integrated artificial neural network and empirical correlations approach to predict critical heat flux for subcooled water. Recently, Naphon and Arisariya-

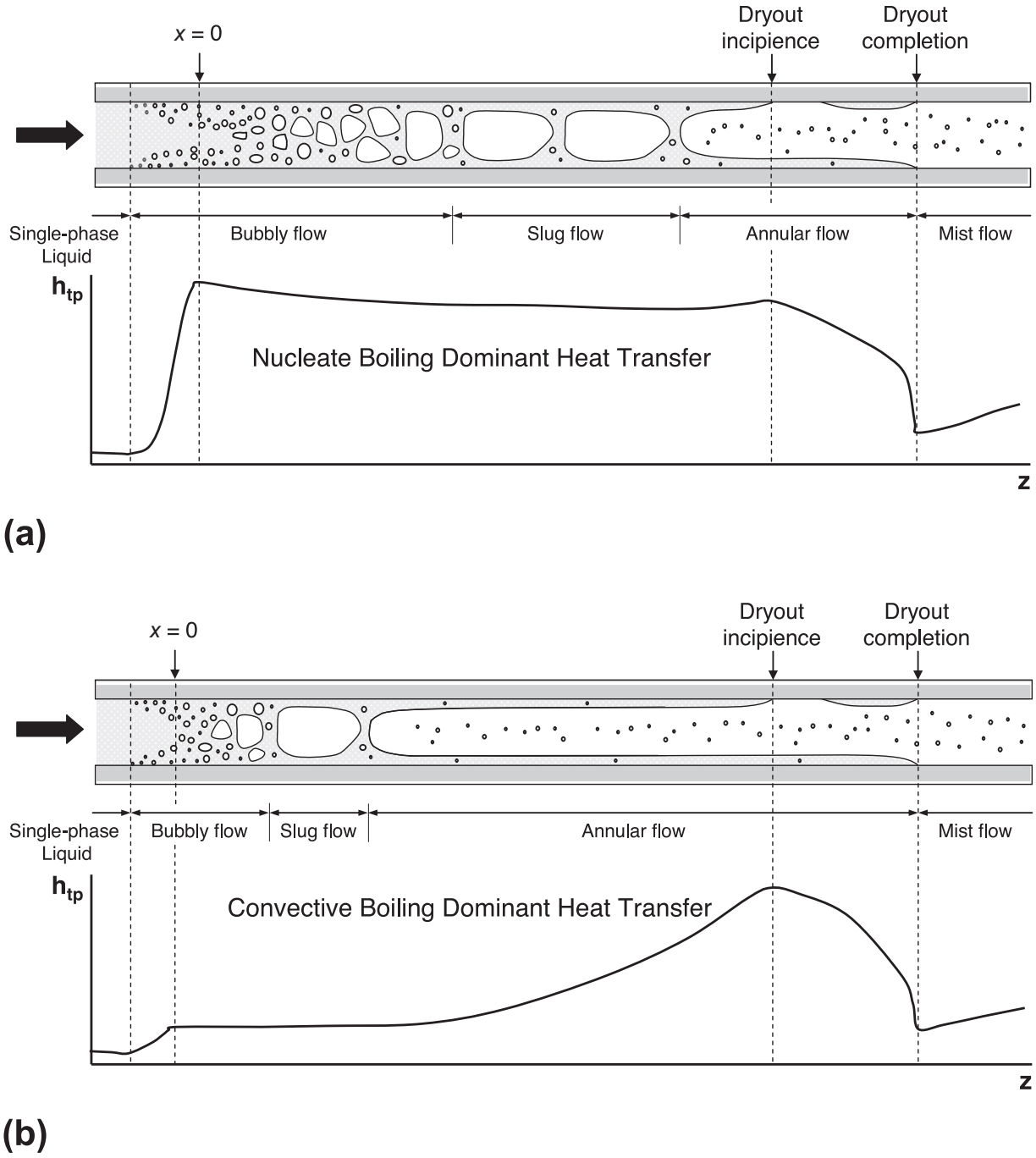

Fig. 2. Schematics of flow regimes, wall dryout and variation of heat transfer coefficient along uniformly heated channel for (a) nucleate boiling dominant heat transfer and (b) convective boiling dominant heat transfer. Adapted from [3].

wong [25] applied ANNs to analyze the heat transfer and friction factor of horizontal tube heat exchanger with spring insert. Their results showed that the ANN could predict the experimental data for heat transfer coefficient and friction factor with errors less than 2.5% and 7.5%, respectively, performing better than available correlations in literature. In addition, Naphon et al. [26] investigated heat transfer and friction factor of spirally fluted tubes showing that their predictions also outperformed available correlations in literature. We are also seeing a lot of work being done on developing ANNs for predicting heat transfer and pressure drop behaviors in nanofluid based flow systems [27–30]. In a study by Naphon et al. [29], ANNs were tested on spirally coiled tubes with four different backpropogation algorithms to develop an optimized model for TiO_2/water nanofluids heat transfer and pressure drop. In another study, Naphon et al. [30] tested jet impingement of nanofluids in microchannel heatsinks to obtain heat transfer and pressure drop data and utilized ANNs and computational fluid dynamics simulations to predict the data. Although ANNs have shown such promise in predicting thermal characteristics across many thermal system applications, ANN methods have not yet been applied to predicting complex systems like saturated flow boiling heat transfer in mini/micro-channels. With the availability of heat transfer coefficient databases as used in universal correlation papers, we now have the capability to develop models based on large datasets, and correlate ANNs for these systems.

Table 1
Saturated flow boiling heat transfer data for mini/micro-channels included in consolidated database [31–80].

Author(s)	Channel geometry[a]	Channel material	D_h (mm)	Relative roughness R, e/D_h	Fluid(s)	G (kg/m^{2}s)	Data points
Wambsganss et al. [31]	C single, H	Stainless steel	2.92	Smooth	R113	50–300	92
Tran (1998)	C single, H	Brass	2.46	Smooth	R134a	33–502	302
Wang et al. [43]	C single, H	Copper	6.5	Smooth	R22	100–400	63
Yan and Lin [54]	C multi, H	Copper	2.0	–	R134a	50–200	137
Bao et al. [65]	C single, H	Copper	1.95	Smooth	R11, R123	167–560	164
Qu and Mudawar [76]	R multi, H	Copper + Lexan cover	0.349	–	Water	135–402	335
Sumith et al. [77]	C single, VU	Stainless steel	1.45	––	Water	23–153	85
Yun et al. [78]	C single, H	Stainless steel	6.0	Smooth	R134a, CO_2	170–340	182
Huo et al. [79]	C single, VU	Stainless steel	2.01, 4.26	0.0009, 0.0004	R134a	100–500	365
Lee and Mudawar [80]	R multi, H	Copper + Lexan cover	0.349	–	R134a	61–657	111
Saitoh et al. [33]	C single, H	Stainless steel	0.51, 1.12, 3.1	Smooth	R134a	150, 300	420
Yun et al. [34]	R multi, H	Stainless steel	1.14, 1.53, 1.54	–	CO_2	200–400	57
Muwanga and Hassan (2007)	C single, H	Stainless steel	1.067	–	FC72	770–1040	454
Zhao and Bansal [36]	C single, H	Stainless steel	4.57	Smooth	CO_2	140–231	22
Agostini et al. [37]	R multi, H	Silicon + Lexan cover	0.336	0.0005	R236fa	281-1370	593
Consolini [38]	C single, H	Stainless steel	0.51, 0.79	0.0047, 0.0022	R134a, R236fa, R245fa	274–1435	650
Bertsch et al. [12]	R multi, H	Copper + Lexan cover	0.544, 1.089	$<$ 0.0009, $<$ 0.0006	R134a, R245fa	19–336	332
In and Jeong [40]	C single, H	Stainless steel	0.19	-	R123, R134a	314–470	256
Mastrullo et al. [41]	C single, H	Stainless steel	6.0	Smooth	CO_2	200–349	143
Ohta et al. [42]	C single, H	Stainless steel	0.51	–	FC72	107, 215	24
Wang et al. [44]	C single, H	Stainless steel	1.3	–	R134a	321–836	365
Ducoulombier [45]	C single, H	Stainless steel	0.529	0.0015-0.0030	CO_2	200–1400	1573
Hamdar et al. [46]	R single, H	Aluminum	1.0	–	R152a	210–580	50
Martín-Callizo [47]	C single, VU	Stainless steel	0.64	0.0012	R134a, R22	185–535	381
Ong [48]	C single, H	Stainless steel	1.03, 2.20, 3.04,	0.0006, 0.0004, 0.0003	R134a, R236fa, R245fa	199–1608	2504
Tibiriçá and Ribatski [49]	C single, H	Stainless steel	2.32	0.0001	R134a, R245fa	50–700	130
Ali et al. [50]	C single, VU	Stainless steel	1.7	0.0001	R134a	75–600	152
Bang et al. [51]	C single, H	Stainless steel	1.73	–	Water	100	65
Copetti et al. [52]	C single, H	Stainless steel	2.62	0.0008	R134a	240–932	876
Mahmoud et al. [53]	C single, VU	Stainless steel	1.1	0.0012	R134a	128–549	152
Oh and Son [55]	C single, H	Stainless steel	4.57	Smooth	CO_2	400–900	107
Oh and Son [56]	C single, H	Copper	1.77, 3.36, 5.35	Smooth	R134a, R22	200–500	153
Wu et al. [57]	C single, H	Stainless steel	1.42	–	CO_2	300–600	419
Costa-Patry & John [58]	R multi, H	Copper	0.295	–	R134a, R245fa, R1234ze	205–569	510
Karayiannis et al. [59]	C single, VU	Stainless steel	1.1	0.0012	R134a	215–550	545
Li et al. [60]	C single, H	Stainless steel	2.0	Smooth	R1234yf, R32	100–400	169
Tibiriçá et al. [61]	C single, H	Stainless steel	1.0, 2.2	0.0006, 0.0004	R1234ze	300–600	30
Balasubramanian et al. [62]	R multi, H	Copper	0.489, 0.504	0.00409, 0.00397	water	88–751	332
Davide Del Col et al. [63]	C single, H	Copper	0.96	0.001354	R134a, R1234yf	200–600	93
Grauso et al. [64]	C single, H	Stainless steel	6	Smooth	R1234ze(E), R134a	270.75–285.25	575
Vakili-Farahani et al. [66]	R multi, VU	Aluminum	1.44	–	R245fa, R1234ze	100–400	138
Charnay et al. [67]	C single, H	Stainless steel	3.0	–	R245fa	300–1500	285
Wang et al. [68]	C single, H	Copper	6.0	Smooth	Propane	63.9–102.8	127
Anwar et al. [69]	C single, VU	Stainless steel	1.6	0.000594	R1234yf	300–500	256
Charnay et al. [70]	C single, H	Stainless steel	3.0	–	R245fa	300–1000	337
Markal et al. [71]	R multi, H	Silicon	0.15	–	Water	51–92.6	20
Xu et al. [72]	C single, H	Copper	0.501, 1.084, 2.0235	–	R134a	185–910	225
Sempértegui-Tapia & Ribatski [73]	C multi, H	Stainless steel	0.868, 1.1	0.0026, 0.0097	R134a	200–800	685
Sempértegui-Tapia & Ribatski [73]	C single, H	Stainless steel	1.1	0.0026	R134a, R600a, R1234yf, R1234ze	200–500	862
Fayyadh et al. [75]	R multi, H	Copper	0.42	0.000716	R134a	50–300	50
Total							16953

[a] C: circular, R: rectangular, H: horizontal, VU: vertical upward.

1.4. Objective of study

A consolidated database consisting of 16953 data points for flow boiling heat transfer in mini/micro-channels is amassed from 50 sources [31–80]. Table 1 provides key information on these individual databases incorporated into the consolidated database. This database includes 13653 single- channel data points from 38 sources, and 3300 multi-channel data points from 12 sources. The consolidated database includes a broad range of two-phase heat transfer coefficient data points with the following coverage:

- Working fluid: CO_2, FC72, Propane, R11, R113, R123, R1234yf, R1234ze, R134a, R152a, R22, R236fa, R245fa, R32, R600a and water
- Reduced pressures: $0.0046 < P_R < 0.77$
- Hydraulic diameter: $0.15\ \text{mm} < D_h < 6.5\ \text{mm}$
- Mass velocity: $19\ \text{kg/m}^2\text{s} < G < 1608\ \text{kg/m}^2\text{s}$
- Liquid-only Reynolds number: $27 < Re_{fo} = GD_h/\mu_f < 55270$
- Flow quality: $0 < x < 1$

The objective of this study is to build an ANN model for predicting heat transfer for flow boiling in mini/micro-channels by utilizing the consolidated experimental data in the whole saturated liquid-vapor domain, including pre and post-dryout heat transfer. A large set of input parameters, including flow, geometric, operating and relevant dimensionless parameters will be used to setup the ANN analysis, and later down-selected to improve the predicting capability. In addition, the predicted results will also be compared with universal correlations to see how the ANN technique compares with that predicting approach. Before concluding this study, the ANN model will be modified to predict datasets that are not included in the model development.

2. ANN

2.1. ANN background

Neural networks were first proposed by McCullough and Pitts in 1943 [81]. An artificial neural network (ANN) is based on a collection of connected units or nodes called artificial neurons. A general ANN architecture consists of an input layer, hidden layers and an output layer through which a set of input parameter are supplied to the input nodes for the feed forward process, and the information is transferred through the network to the nodes in the output layer. ANN is a powerful universal approximator with which it can create mapping of one vector onto another vector space [82]. The power of ANN lies in the fact that it can capture some a priori hidden relation in the input data albeit without extracting it. Capturing the information hidden in the data is called as “Training the Neural Networks” [83].

The basic computation unit in ANN is a neuron as shown in Fig. 3(a), where a weighted sum of input signals to a neuron is passed through an activation function, f, to produce an output signal. Since a neuron itself is a non-linear unit, neural networks are also non-linear [83]. There are different choices of activation functions, for e.g., Sigmoid function, hyperbolic tangent function, and rectified linear unit (ReLu) function as shown in Fig. 3(b). ReLu function is the most popular out of these because the conventional activation functions like sigmoid and hyperbolic tangent suffer from the vanishing gradient problem [84]. ReLu activation functions greatly accelerates the convergence of gradient descent due to its linear, non-saturating form [84].

For the present work a multi-layer feed forward neural network is developed in which all the nodes of a layer are connected to all other nodes of the preceding and following layers. With such dense connection between the nodes, the ANN learns to predict the desired output supplied during the training process. The output from such a network is an explicit function of inputs and biases and does not require any feedback loops [85]. Since the output from such a network is a continuous real number, it is equivalent to solving a regression problem in which the loss function is defined as a sum of squared error.

ANN have many advantages that make it suitable for applying to complex systems like saturated flow boiling. Today, training ANN can be achieved easily for such systems because of the significant computational power capability. ANN model can be easily scaled up if additional data points for new fluids/operating conditions become available. ANN have the property that output can be expressed as a deterministic function of input, thereby representing a multivariate non-linear function mapping. Hence, ANN do not explore the underlying physics of the problem but learn the pattern from the data available making them different from the traditional techniques. A neuron, part of the ANN network, is a non-linear unit, and consequently, ANN is non-linear which learns non-linearity in the data points without any assistance from the user. On the other hand, ANN also suffer from a few disadvantage specific to the current system. Usually, ANNs need many data points for training. The number of data points used in this study are 16,953 while traditional ANNs are trained through millions of data points, which is not viable in this situation. In addition, on applying ANN outside the convex hull of the training data, the performance of the ANN is generally poor, consequently giving large error values. This is because the absence of the data in the training set provides no basis of providing any prediction value. Predictions are also inaccurate if there is a large void inside the training set due to the absence of data. Traditional techniques many times have the ability to capture the information outside the range because they are based on the underlying physics.

2.2. Backpropagation algorithm

ANNs utilize learning algorithms, and the most widely used algorithm for ANN with differential activation functions is the backpropagation algorithm during which the input signal is transmitted forward through a transfer function and the errors are propagated backwards. The technique of backpropagation was popularized by Rumelhart et al. [86], which is depicted in Fig. 3(c). The objective function or the loss function to be used for the backpropagation algorithm is chosen to be Mean Square Error (*MSE*). *MSE* is a differentiable function and is a commonly used metric in regression problems, with the difference being that in regression problems, it is explicit, while in backpropagation algorithm, it is implicit [87]. The backpropagation algorithm is used to find the local minimum of the loss function, where the gradient of the loss function for the output layer and the hidden layer is calculated recursively.

Consider a network with M training examples, n input parameters, and a total of L layers (including input and output layer). $w_{ij}^{l}$is the weight connecting node i in layer $(l-1)$ to node j in layer (l),$d^{l}$is the number of nodes at layer (l), and S_{mj}^{l} is the output. The value of parameter $x_{mj}$for node $j$in layer (l) is computed as

$$x_{mj} = f(S_{mj}^{l}), \tag{1}$$

$$\text{where} \quad S_{mj}^{l} = \sum_{i=1}^{d^{l-1}} w_{ij}^{l} x_{mi}^{l-1}, \tag{2}$$

$$\text{and} \quad \frac{\partial S_{mj}^{l}}{\partial w_{ij}^{l}} = x_{mi}^{l-1}. \tag{3}$$

For the mth training example, the loss function,E_m, is defined by the square of the Euclidean distance between the network output

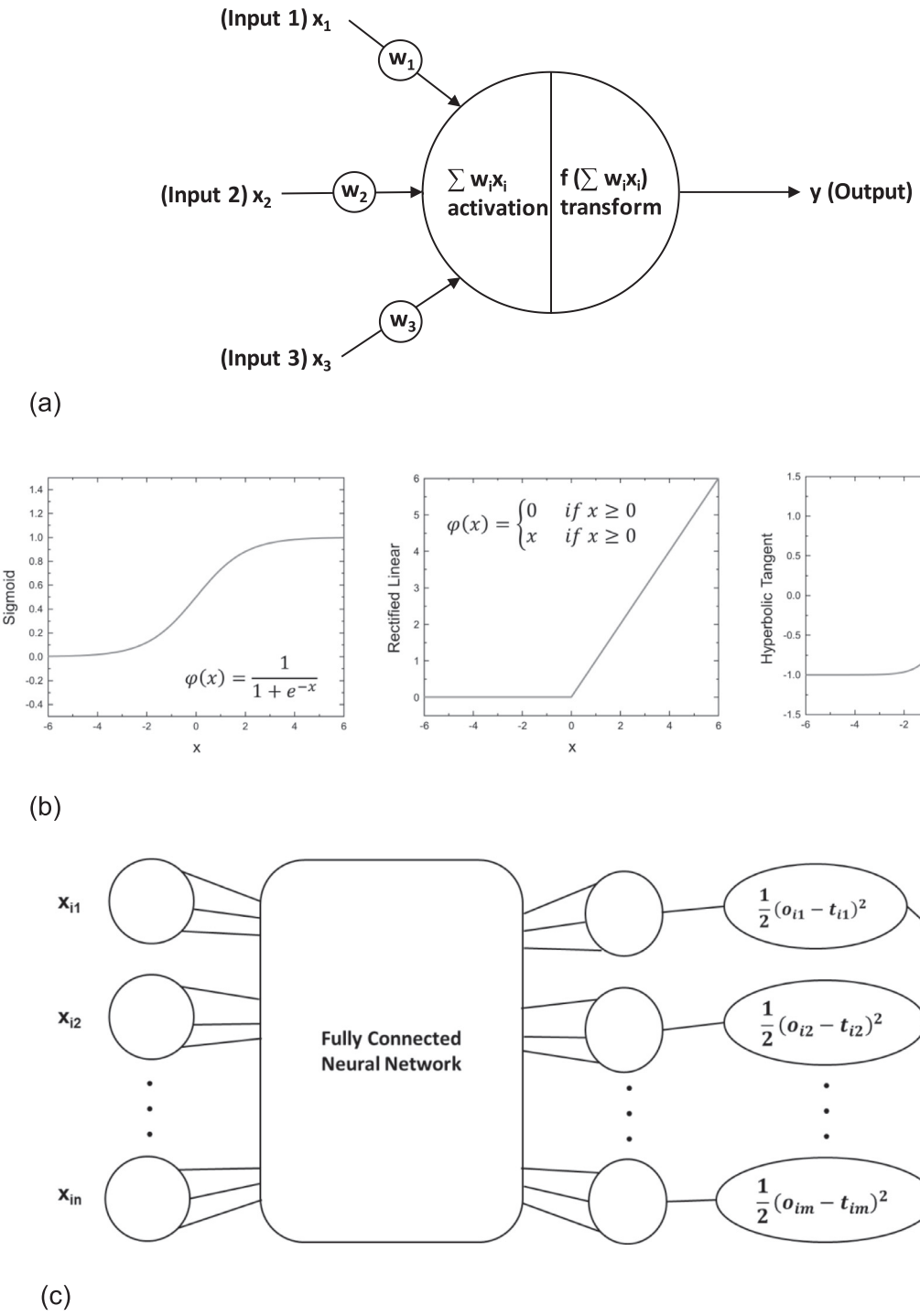

Fig. 3. (a) A single neuron. (b) Common activation functions. (c) Backpropagation algorithm.

vector and target vector given by

$$E_m = \frac{1}{2}\left\| f\left(S_{mj}^L\right) - t_m \right\|^2, \tag{4}$$

where $t_m$is the target value of the mth example. Each of the nodes j in the last hidden layer is connected to the output node and contributes to Eq. (4).

If we differentiate Eq. (4) with respect to the error at the outermost node, ${\delta_{mj}}^L$, we get

$$\frac{\partial E_m}{\partial \delta_{mj}^L} = \frac{\left(f\left(S_{mj}^L\right) - t_m\right) f'\left(S_{mj}^L\right)}{\partial \delta_{mj}^L}, \tag{5}$$

where

$$\delta_{mj}^L = \frac{\partial E_m}{\partial S_{mj}^L} = \frac{\partial E_m}{\partial f\left(S_{mj}^L\right)} \frac{\partial f\left(S_{mj}^L\right)}{\partial S_{mj}^L} = f\left(S_{mj}^L\right) - t_m. \tag{6}$$

Since the activation function f is ReLu given as

$$f(x) = \begin{Bmatrix} x, x \geq 0 \\ 0, x < 0 \end{Bmatrix}, \tag{7}$$

the differential f' is given as

$$f' = \begin{cases} 1 \; if \; S_m^L \geq 0 \\ 0 \; otherwise \end{cases}. \tag{8}$$

Gradient of the loss function with respect to weight is computed as

$$\frac{\partial E_m}{\partial w_{ij}^L} = \frac{\partial E_m}{\partial S_{mj}^L} \times \frac{\partial S_{mj}^L}{\partial w_{ij}^L} = \delta_{mj}^L \times \frac{\partial S_{mj}^L}{\partial w_{ij}^L} = \delta_{mj}^L x_{mi}^{(L-1)}. \quad (9)$$

The total error of the training set, E, is the summation of all the quadratic errors and is given as

$$E = \sum_{m=1}^{M} E_m = \frac{1}{2}\sum_{m=1}^{M} \left\| f\left(S_{mj}^L\right) - t_m \right\|^2. \quad (10)$$

By computing δ_{mj}^L, we can compute the gradient of the error with respect to the weight at every node,

$$\frac{\partial E}{\partial w_{ij}^L} = \sum_{m=1}^{M} \frac{\partial E_m}{\partial w_{ij}^L} = \sum_{m=1}^{M} \delta_{mj}^L x_{mi}^{(L-1)}, \quad (11)$$

Each weight in the network,w_{ij}^l, is further updated using the following operation:

$$w_{ij}^l = w_{ij}^l - \lambda \frac{\partial E}{\partial w_{ij}^l}, \quad (12)$$

where i = 1,2,3,... L-1, and λ is the learning rate. To get a final solution, E can be minimized by solving for weights using an iterative process of gradient descent algorithm [86].

2.3. Neural network model selection

It's well known that a neural network is considered a black-box which does 'not provide any insight about the features of the system [88]. In this study, different neural network architectures were tested. The most optimal network architecture depends on several factors like the number of training cases, number of input parameters, amount of noise in the data, activation function, regularization parameter and the loss function [83]. A neural network with few hidden layer is not capable of learning training data; therefore, the accuracy of the system is limited. On the contrary, an over-fitting problem may be obtained if the network has a greater depth (large number of hidden layers), and again, the performance of the system is limited.

The code is written in Python, and Pandas, Numpy and Scikit-learn libraries were used to develop the model. The input parameters were standardized to a Gaussian like distribution with zero mean value and unit variance. Although there are sophisticated methods of weight initialization like orthogonal least square algorithm [89], for the present work, network is initialized with randomly assigned weights. The resulting data set was split into training and test datasets with 75% – 25% split ratio with 12624 training data points and 4239 test data points. Data partitioning was investigated before selecting this data split ratio.

Table 2 shows the different ANN model parameters optimized and selected in this study. As seen in the table, the learning rate, λ, is set to 0.001 . A larger value of learning rate may accelerate convergence but have the chances of oscillation near the optimum point. To prevent overfitting, the L2 regularization parameter (α_r) is set to 0.001. The optimization algorithm used is Adam [90] instead of standard gradient descent algorithm as the former has better performance over latter due to adaptive learning rate. The exponential decay rate of the first and second moments is specified to be 0.9 and 0.999, respectively.

Table 2
ANN model parameters selected in this study.

Parameter	Value
Activation function	ReLu
L2 Regularization Parameter, α	0.001
Solver	Adam
Batch size	200
Learning rate, λ	0.001
Exponential decay rate for estimates of first moment vector, $\beta 1$	0.9
Exponential decay rate for estimates of second moment vector, $\beta 2$	0.999
Tolerance	0.001

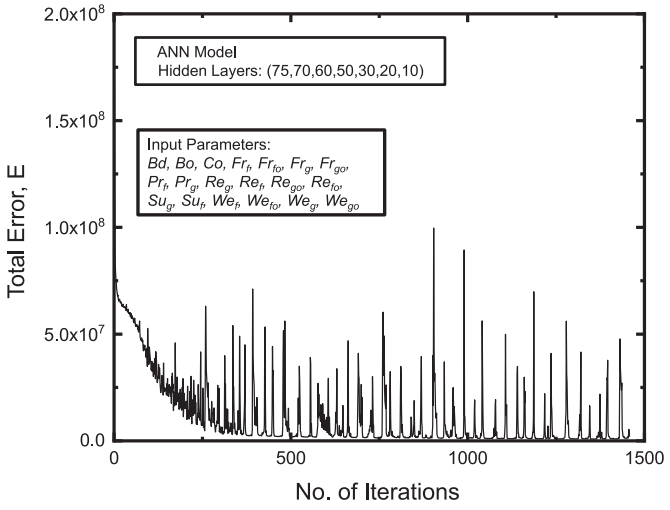

Fig. 4. MSE total error function variation with number of iterations for ANN model with hidden layers (75,70,60,50,30,20,10) and input parameters of Bd, Bo, Co, Fr_f, Fr_{fo}, Fr_g, Fr_{go}, Pr_f, Pr_g, Re_g, Re_f, Re_{go}, Re_{fo}, Su_g, Su_f, We_f, We_{fo}, We_g, and We_{go}.

2.4. Neural network error estimation

The loss function to minimize is *MSE* loss, as it is the preferred loss function under the inference framework of maximum likelihood [91]. As stated in [92], backpropagation algorithm cannot be shown to converge and there are no clear criterion to stop its operation. For the present study, the Adam optimizer is run until the *MSE* loss is minimized with maximum number of iterations to not meet tolerance (0.001) is 100. As shown in Fig. 4, the plot shows the change in *MSE* loss with iterations for the ANN network depicted in Fig. 5. When deemed to be converged, the iterations are stopped if the change in *MSE* loss is within the specified tolerance. The spikes seen during iterations are due to the fact that training examples are converged with batch size of 200. Stochastic gradient descent, on the other hand, converges each training example individually and hence has a nosier convergence history.

The accuracy of models is ascertained mainly using mean absolute error (*MAE*), which is defined as

$$MAE = \frac{1}{N}\sum \frac{\left|h_{\mathrm{tp,pred}} - h_{tp,exp}\right|}{h_{tp,exp}} \times 100\% \quad (13)$$

Also used to understand model predictions are parameters θ, which is the percentage data predicted within ±30%, and ε, which is the percentage data predicted within ±50%. Many studies with ANN for analyzing thermal systems use R-squared error (coefficient of determination or R^2) which will also be used for understanding model predictability. R^2 is preferred over R (Pearson's correlation coefficient) as the former usually measures the linear correlation coefficient while the latter provides the measure for the proportion of variance explained by the model and is independent of the scale of dependent variable [93]. R^2 is defined as

$$R^2 = 1 - \frac{\sum\left(h_{\mathrm{tp,exp}} - h_{tp,pred}\right)^2}{\sum\left(h_{\mathrm{tp,exp}} - \bar{h}_{tp,\mathrm{exp}}\right)^2}. \quad (14)$$

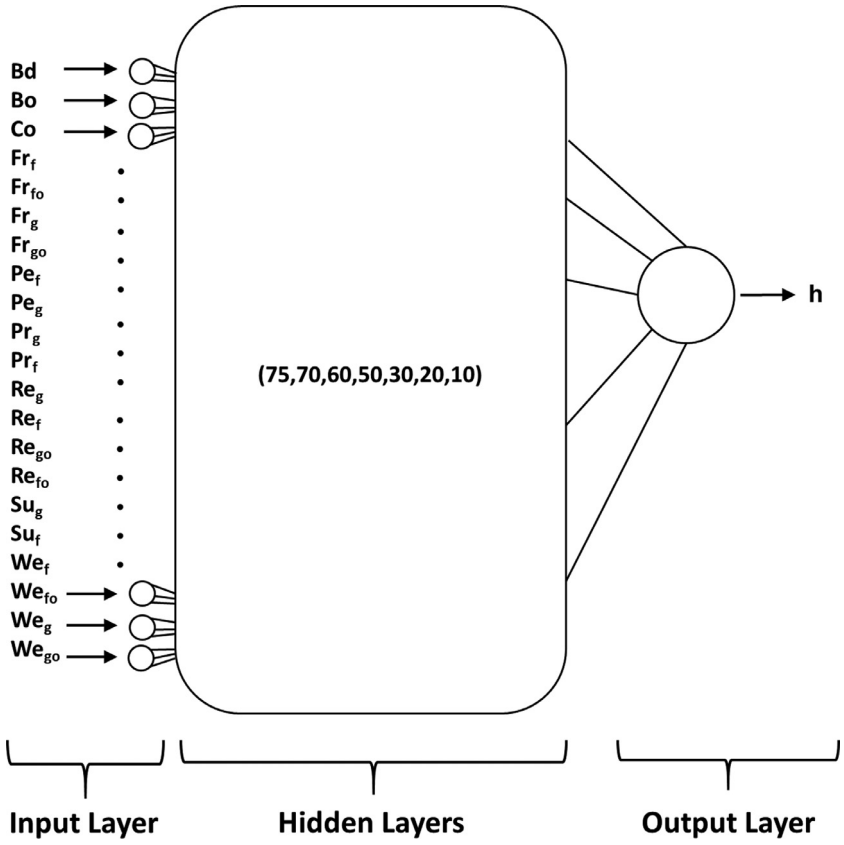

Fig. 5. ANN architecture with input, hidden and output layers selected as the final model for this study

Table 3
ANN model predictions for fixed hidden layers and different combinations of input parameters.

Test Case	ANN Model Hidden Layers	Input Parameters	MAE (%)	R^2	Θ (%)	E (%)
1	(75,70,60,50,30,20,10)	*Bo, Bd, Re_f, Re_g*	33.11%	0.47	59.09%	82.12%
2		*Fr_f, Pr_f, Re_f, Su_f, We_f*	39.42%	0.55	59.66%	80.56%
3		*Fr_g, Pr_g, Re_g, Su_g, We_g*	36.45%	0.15	68.60%	85.70%
4		*Fr_f, Fr_{fo}, Pr_f, Re_f, Re_{fo}, Su_f, We_f, We_{fo}*	28.25%	0.52	73.77%	88.44%
5		*Fr_g, Fr_{go}, Pr_g, Re_g, Re_{go}, Su_g, We_g, We_{go}*	27.00%	0.86	76.32%	90.26%
6		*q", T, x*	38.59%	0.41	62.61%	79.88%
7		*D, G, P, P_c, q", x*	20.02%	0.88	82.59%	93.25%
8		*P, P_c, D, G, x, q", R, ρ_g, ρ_f, h_{fg}, c_{vg}, c_{vf}, c_{pg}, c_{pf}, μ_g, μ_f, σ*	13.69%	0.82	92.64%	97.45%
9		*Bd, Bo, Co, c_{pg},c_{pf}, c_{vg}, c_{vf}, D, Fr_f, Fr_{fo}, Fr_g, Fr_{go}, G, h_{fg}, k_f, k_g, P_c, P_F, P_H, Pe_f, Pe_g, P, Pr_f, Pr_g, q", R, Re_f, Re_{fo}, Re_g, Re_{go}, Su_f, Su_g, T, We_f, We_{fo}, We_g, We_{go}, Xtt, x β, μ_f, μ_g, ρ_f, ρ_g, σ*	15.29%	0.77	91.53%	97.26%
10		***Co, Bd, Bo, Fr_f, Fr_{fo}, Fr_g, Fr_{go}, Pr_f, Pr_g, Re_f, Re_{fo}, Re_g, Re_{go}, Su_f, Su_g, We_f, We_{fo}, We_g, We_{go}****	14.30%	0.83	92.00%	97.38%

* Final selected model configuration.

3. Results and discussion

3.1. ANN model selection

The consolidated data is utilized to test, develop, and compare ANN models based on different combinations of input parameters and hidden layers to evaluate the impact of selecting specific input parameters on model's heat transfer coefficient predicting capability.

In Table 3, for a fixed ANN model with hidden layers set to (75,70,60,50,30,20,10), we compare the predicting capability with different combinations of operating, geometric, and dimensionless input parameters. As we can see in Fig. 6(a), a model utilizing very few input parameters namely, *Bd, Bo, Re_g, and Re_f,* is not able to predict the test data very well and shows an *MAE* of 33% and R^2 of 0.47 on the test dataset. This shows that we have selected fewer parameters that those necessary to capture the trends of heat transfer coefficient in saturated flow boiling and therefore, further improvement is necessary. The effect of selecting only liquid or gas parameters on heat transfer coefficient predicting ability of the model was also examined. The reason to do this is to verify that two-phase behavior cannot be predicted with knowledge of only the single-phase parameters. As can be seen in Table 3, for liquid parameters: Fr_f, Pr_f, Re_f, Su_f, and We_f, and for gas parameters: Fr_g, Pr_g, Re_g, Su_g, and We_g, the predicting capability is not improved and shows a deteriorated *MAE* of 39.4% and 36.5%, respectively. On the other hand, if we include the effect of channel dimensions by adding the gas only dimensionless numbers in the gas based model, the predicting capability improves slightly as we can see with input parameters of Fr_g, Fr_{go}, Pr_g, Re_g, Re_{go}, Su_g, We_g, and We_{go}, where the *MAE* is now 27.0%. Similarly, for the fluid based model input parameters, Fr_f, Fr_{fo}, Pr_f, Re_f, Re_{fo}, Su_f, We_f, and

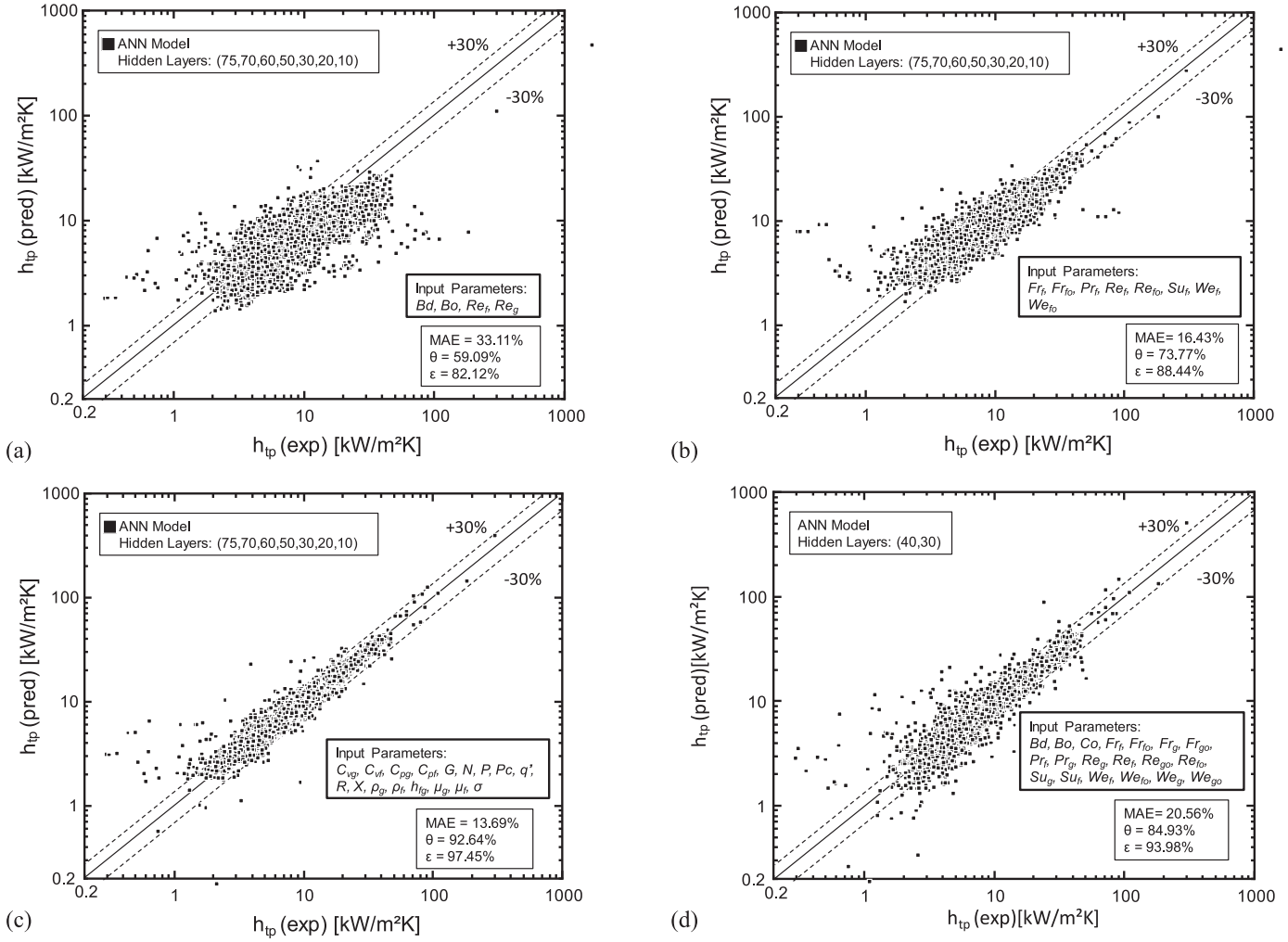

Fig. 6. ANN model predictions of 4239 test data points for (a) hidden layers (75,70,60,50,30,20,10) and input parameters Re_g, Re_f, Bo, and Bd, (b) hidden layers (75,70,60,50,30,20,10) and input parameters Fr_f, Fr_{fo}, Pr_f, Re_f, Re_{fo}, Su_f, We_f, and We_{fo}, (c) hidden layers (75,70,60,50,30,20,10) and input parameters C_{vg}, C_{vf}, C_{pg}, C_{pf}, D_h, G, P, P_c, q", R, T, x, ρ_g, ρ_f, h_{fg}, μg, μ_f, and σ, and (d) hidden layers (40,30) and input parameters Bd, Bo, Co, Fr_g, Fr_{go}, Fr_f, Fr_{fo}, Pr_g, Pr_f, Re_g, Re_{go}, Re_f, Re_{fo}, Su_g, Su_f, We_g, We_{go}, We_f, and We_{fo}.

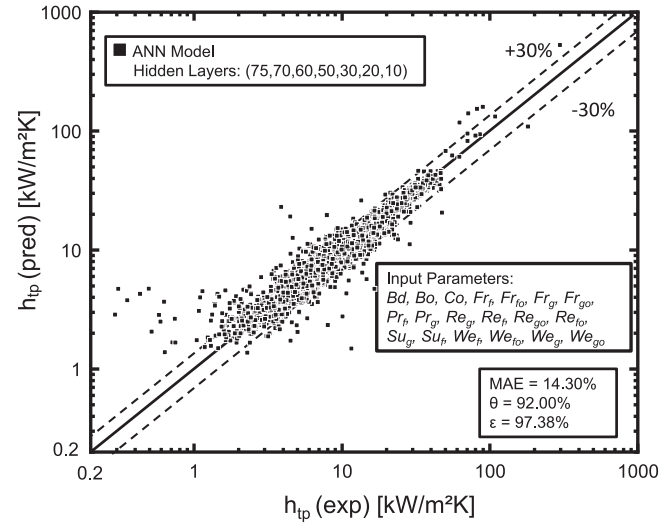

Fig. 7. Comparison of predicted 4239 test data points and the corresponding experimentally measured heat transfer coefficients data for final selected ANN model with hidden layers (75,70,60,50,30,20,10) and input parameters Bd, Bo, Co, Fr_f, Fr_{fo}, Fr_g, Fr_{go}, Pr_f, Pr_g, Re_g, Re_f, Re_{go}, Re_{fo}, Su_g, Su_f, We_f, We_{fo}, We_g, and We_{go}.

We_{fo}, the prediction is also improved with *MAE* of 25.3%. The comparison between predicted and experimental heat transfer coefficients for the fluid based model is shown in Fig. 6(b). We can also see in Table 3, how geometric and operating parameters can directly be utilized to develop models with varying capability similar to what is observed with dimensionless numbers. A model which utilizes as input parameters, c_{vg}, c_{vf}, c_{pg}, c_{pf}, D_h, G, P, P_c, q", R, T, x, ρ_g, ρ_f, h_{fg}, μg, μ_f, and σ, performs the best with the lowest *MAE* of 13.7% amongst all models, and the comparison between experimental and predicted data for this model is shown in Fig. 6(c). For this model the R^2 is also high at 0.82. Let us now consider a model which uses input parameters based on all dimensionless parameters relevant to two-phase saturated boiling, namely, *Bd, Bo, Co, Fr_g, Fr_{go}, Fr_f, Fr_{fo}, Pr_g, Pr_f, Re_g, Re_{go}, Re_f, Re_{fo}, Su_g, Su_f, We_g, We_{go}, We_f,* and *We_{fo}*. This model as we can see in Fig. 7 does a reasonably good job at predicting the test data with *MAE* of 14.3% and R^2 of 0.83. Even though it was observed that a model utilizing only geometric and operating parameters performed slightly better as shown in Fig. 6(c), we will select the completely dimensionless model as our final model in this study. Staying with dimensionless parameters is important in developing generalized predicting tools in two-phase flow situations.

Also optimizable for improving the predicting capability is the number of hidden layers in the ANN model. Hidden layers are

Table 4
ANN model predictions for fixed input parameters and different combinations of hidden layers.

Test Case	ANN model hidden layers	Input parameters	MAE (%)	R^2	θ (%)	ε (%)
1	(95,85,75,70,60,50,30,20,10)	*Co, Bd, Bo, Fr_f, Fr_{fo}, Fr_g,*	14.44%	0.87	91.48%	96.56%
2	(80,75,70,60,50,30,20,10)	*Fr_{go}, Pr_f, Pr_g, Re_f, Re_{fo},*	17.15%	0.87	89.55%	96.25%
3	**(75,70,60,50,30,20,10)***	*Re_g, Re_{go}, Su_f, Su_g, We_f,*	14.30%	0.83	92.00%	97.38%
4	(70,60,50,30,20,10)	*We_{fo}, We_g, We_{go}*	15.95%	0.89	90.94%	96.04%
5	(60,50,30,20,10)		17.25%	0.91	88.37%	95.90%
6	(50,30,20,10)		19.78%	0.95	84.64%	94.17%
7	(50,30,20)		18.41%	0.92	87.87%	95.23%
8	(40,30,20)		23.67%	0.75	81.91%	99.69%
9	(40,30)		20.56%	0.86	84.45%	94.00%
10	(30,20)		23.81%	0.72	79.71%	91.86%
11	(40)		28.45%	0.44	74.14%	87.97%
12	(20)		31.03%	0.41	71.86%	86.91%

* Final selected model configuration.

Table 5
Previous universal/generalized saturated flow boiling heat transfer correlations [1,12,13].

Author(s)	Equation	Remarks
Bertsch et al.	$h_{tp} = h_{nb} \cdot S + h_{cb} \cdot F$, $S = 1 - x$, $F = 1 + 80(x^2 - x^6)e^{-0.6C}$, $C = \sqrt{\frac{\sigma}{g(\rho_f - \rho_g)D_h^2}}$ $h_{nb} = 55P_R^{0.12}(-log_{10}P_R)^{-0.55}M^{-0.5}q_H''^{0.67}$, $h_{cb} = h_{cb,fo}(1-x) + h_{cb,go}x$ $h_{cb,fo} = (3.66 + \frac{0.0668\frac{D_h}{L}Re_{fo}Pr_f}{1+0.04(\frac{D_h}{L}Re_{fo}Pr_f)^{2/3}})\frac{k_f}{D_h}$, $h_{cb,go} = (3.66 + \frac{0.0668\frac{D_h}{L}Re_{go}Pr_g}{1+0.04(\frac{D_h}{L}Re_{go}Pr_g)^{2/3}})\frac{k_g}{D_h}$,	D_h = 0.16 – 2.92 mm, G = 20 – 3000 kg/m^{2}s Working fluid: water, nitrogen, methanol, pentane, heptane, benzene, FC-77, R11, R113, R12, R123, R134a, R141b, R236fa, R245fa, R410A 3899 data points
Kim & Mudawar	$h_{tp} = (h_{nb}^2 + h_{cb}^2)^{0.5}$, $h_{nb} = [2345(Bo\frac{P_H}{P_F})^{0.7}P_R^{0.38}(1-x)^{-0.51}](0.023\mathrm{Re}_f^{0.8}\,\mathrm{Pr}_f^{0.4})\frac{k_f}{D_h}$, $h_{cb} =$ $[5.2(Bo\frac{P_H}{P_F})^{0.08}We_{fo}^{-0.52}(1-x)^{-0.51} + 3.5(\frac{1}{X_{tt}})^{0.94}(\frac{\rho_g}{\rho_f})^{0.25}](0.023\mathrm{Re}_f^{0.8}\,\mathrm{Pr}_f^{0.4})\frac{k_f}{D_h}$,	D_h = 0.19 – 6.5 mm, G = 19 – 1608 kg/m^{2}s, Re_{fo} = 57 – 49820 P_R = 0.005 – 0.69 Working fluid: water, CO_2, FC-72, R11, R113, R123, R1234yf, R1234ze, R134a, R152a, R22, R236fa, R245fa, R32, R404A, R407C, R410A, R417A 10805 data points
Fang et al.	$h_{tp} = \frac{k_l}{D}F_f M^{-0.18}Bo^{0.98}Fr_{lo}^{0.48}Bd^{0.72}(\frac{\rho_l}{\rho_g})^{0.29}[\ln(\frac{\mu_{lf}}{\mu_{lw}})]^{-1}Y$, $Y = \begin{cases} 1 & for\ P_R \le 0.43 \\ 1.38 - P_R & for\ P_R > 0.43 \end{cases}$,	D_h = 0.207 – 32 mm, G = 100 – 1782 kg/m^{2}s P_R = 0.0045 – 0.9300 Working fluid: water, CO_2, nitrogen, ammonia, R123, R1234yf, R1234ze, R134a, R152a, R22, R236fa, R245fa, R290, R32, R404A, R410A, R407C, R417A, R507, R600a, R717, R718, R728, R744 17778 data points

crucial in ANN as during back propagation, learning hidden neurons can discover the salient features characterizing the training data [89]. The procedure to select the network architecture mainly depends on the data volume, input variables available and target variable distribution with predictors. The number of nodes in each layer is selected heuristically as there is no rule of thumb that dictates the network width and depth. Usually, the number of layers in the first input layer is more, and then we select the network architecture that tapers down as we have only one output parameter.

As shown in Table 4, for fixed input parameters finalized above, different combinations of hidden layers provide different *MAE*s. For simple models with only one hidden layer, (20) and (40), the *MAE*s are 31.0% and 28.5%, respectively. For these models, the R^2s are 0.41 and 0.44, respectively. As we increase the number of hidden layers, even models with (40,30) and (50,30,20,10) do a good job with the *MAE*s shown as 20.6% and 19.8%, respectively. For (50,30,20,10), the R^2s is as high as 0.95. The comparison between predicted and experimental heat transfer coefficients for the ANN model with hidden layers (40,30) is shown in Fig. 6(d). With significant increase in the number of hidden layers, the model reaches an optimal value for hidden layers of (75,70,60,50,30,20,10), which is selected as the final model in this study. Increasing the number of hidden layers further leads to overfitting in which the *MAE* in the test set increases, thus not providing any further benefit in predicting capability.

Based on this optimization, the ANN model with the dimensionless input parameters: *Bd, Bo, Co, Fr_g, Fr_{go}, Fr_f, Fr_{fo}, Pr_g, Pr_f, Re_g, Re_{go}, Re_f, Re_{fo}, Su_g, Su_f, We_g, We_{go}, We_f,* and *We_{fo}*, and hidden layers (75,70,60,50,30,20,10) will be utilized in this study for predicting the consolidated data as depicted in Fig. 5. With the final model predictions shown in Fig. 7, we can see that the ANN model gives an *MAE* of 14.3% and percentage data predicted within ±30% is 92.0% and percentage data predicted within ±50% is 97.4%.

3.2. ANN comparison with universal correlations

The ANN model results based on the test dataset were compared with predictions of the universal corrections by Bertsch et al. [12], Kim and Mudawar [3], and Fang et al. [13]. Table 5 provides a summary of these universal/generalized saturated flow boiling heat transfer correlations. As we can see in Fig. 8(a), the *MAE* for Bertsch et al. [12] is 46.3% and percentage data predicted within ±30% is 23.6% and percentage data predicted within ±50% is 55.8%. Because the generalized correlation was developed for a smaller range of parameters than those predicted in this study, it is not unreasonable for the overall performance to be low. In Fig. 8(b), we can see that the *MAE* for Kim and Mudawar [3] is 27.4% and the percentage data predicted within ±30% is 75.3% and percentage data predicted within ±50% is 92.4%. It should be noted that Kim and Mudawar [3] only predicts the pre-dryout heat transfer coefficient data because we discard the post-dryout data based on

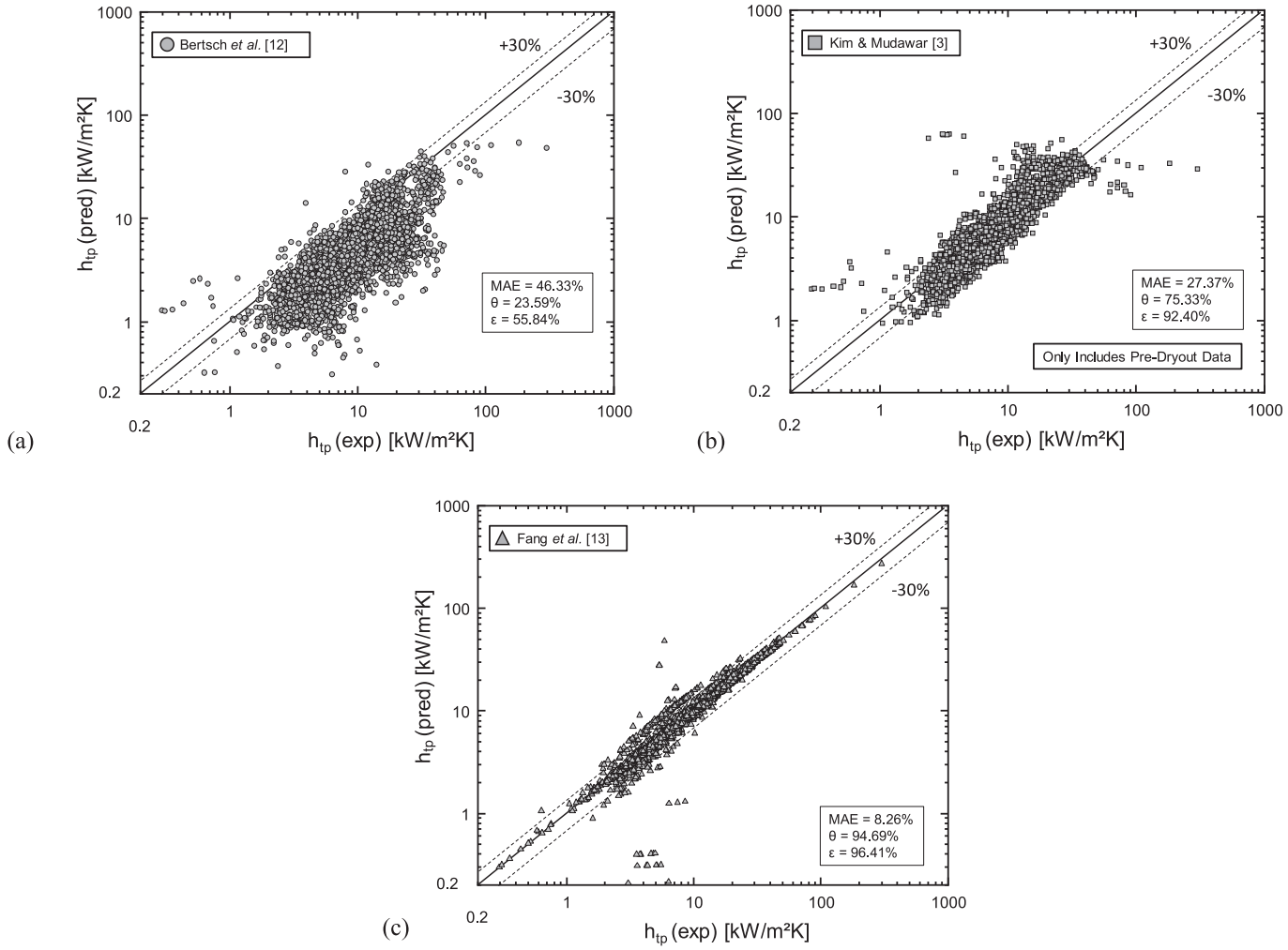

Fig. 8. Comparison of test data points with predictions of previous universal correlations for saturated flow boiling heat transfer by (a) Bertsch et al. [12], (b) Kim and Mudawar [3], and (c) Fang et al. [13].

the dryout incipience quality predicted by Kim and Mudawar [94]. The ANN model predicting capability as shown in Fig. 7 is superior to the correlations by Bertsch et al. [12] and Kim and Mudawar [3]. In Fig. 8(c), we can see that correlation by Fang et al. [13] performs significantly better than both the ANN model and the correlations by Bertsch et al. [12] and Kim and Mudawar [3]. While this shows that the correlation predicting capability is very good, the correlation is not as reliable because it uses information of the inner wall surface temperature to calculate the fluid viscosity in the relationship

$$h_{tp,Fang} = \frac{k_l}{D} F_f M^{-0.18} Bo^{0.98} Fr_{lo}^{0.48} Bd^{0.72} \left(\frac{\rho_l}{\rho_g}\right)^{0.29} \left[\ln\left(\frac{\mu_{lf}}{\mu_{lw}}\right)\right]^{-1} Y, \tag{15}$$

$$\text{and} \quad Y = \begin{cases} 1 & for\, P_R \le 0.43 \\ 1.38 - P_R & for\, P_R > 0.43 \end{cases}, \tag{16}$$

where k_l is the liquid conductivity, F_f a fluid-dependent parameter, M is the molecular mass, and μ_{lf} and μ_{lw} are the liquid dynamic viscosities based on the fluid temperature and the inner wall surface temperature, respectively. As we can see, the correlation uses a viscosity ratio based on the inner wall surface temperature and saturation temperature, which indirectly gives away information about the surface temperature, and therefore the heat transfer coefficient. Going forward, we will only use the correlation by Kim and Mudawar [3] because of both its reliability and high predictability in comparison to other available correlations in predicting saturated flow boiling heat transfer coefficients.

Another important measure of the predicting model capability is its ability to capture individual databases with high accuracies. Fig. 9(a)–(h) shows the model predictions vs. experimental data for the eight largest databases used in the consolidated data. Ong [48] which was the largest database including three working fluids, R134a, R236fa, and R245fa, has *MAE* of 12.5%, and the percentage data predicted within ±30% is 95.2% and percentage data predicted within ±50% is 99%. Similarly, Ducoulombier [45] based on CO2 has *MAE* of 12.7% with, and the percentage data predicted within ±30% is 91.1% and percentage data predicted within ±50% is 96.9%. In general, all eight databases did well and this can be attributed to the ability of ANN model being able to learn and predict the test data better when more training data is provided. These databases include a wide variation of geometric and operating parameters with 7 working fluids: R134a, R1234ze, R236fa, R245fa, R600a, R1234yf, CO_2, mass velocity: 146 – 1608 kg/m²s, hydraulic diameter: 0.34 – 6mm, reduced pressure: 0.05 – 0.47 bar, quality: 0 – 0.99, and fluid only Reynolds number: 419 – 20272. The ANN model predictions were observed to be superior to the universal correlation by Kim and Mudawar [3]. While both techniques have their own significance, the new developed ANN model shows very promising results.

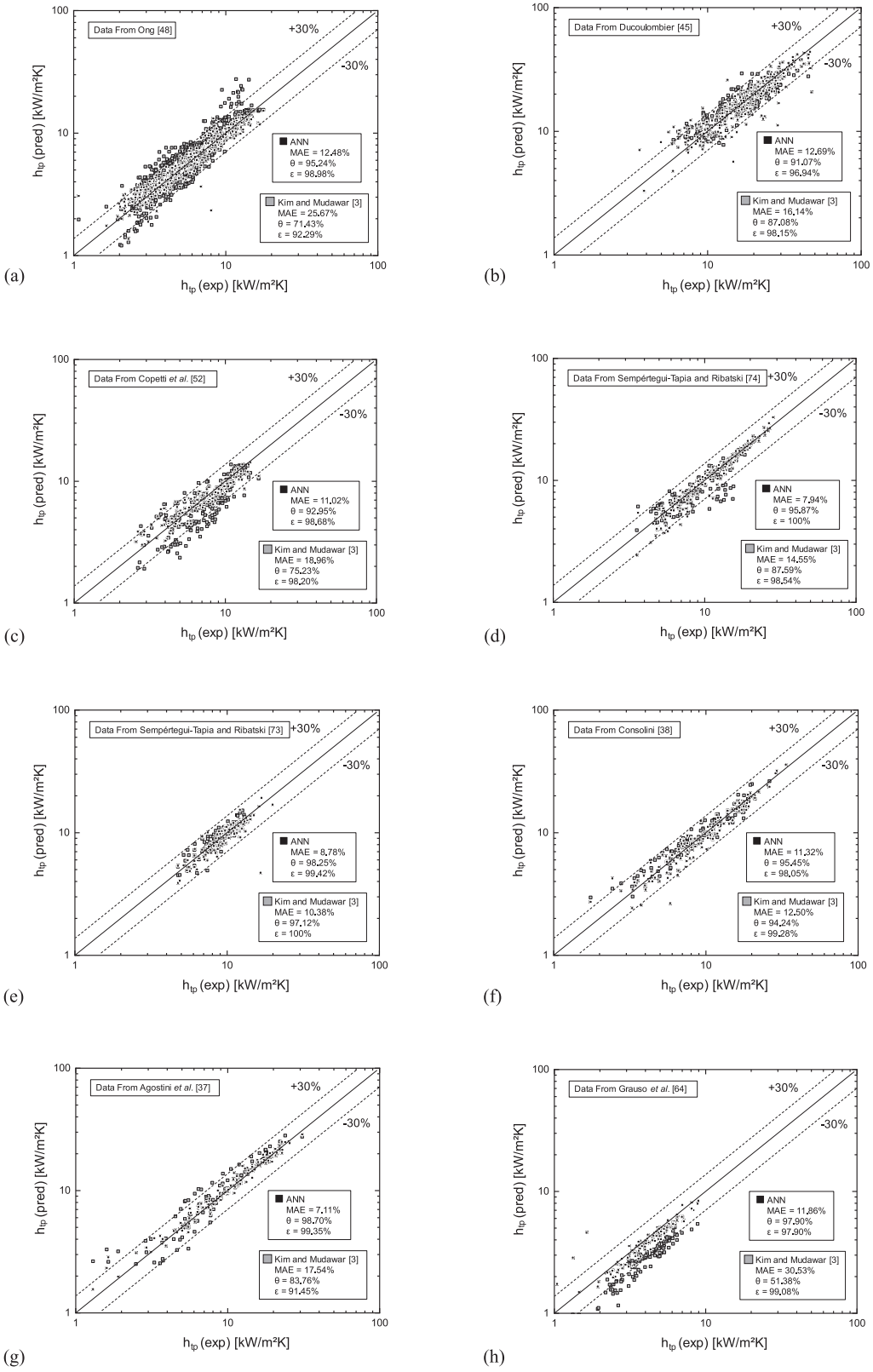

Fig. 9. ANN model with hidden layers (75,70,60,50,30,20,10) and input parameters Bd, Bo, Co, Fr_f, Fr_{fo}, Fr_g, Fr_{go}, Pr_f, Pr_g, Re_g, Re_f, Re_{go}, Re_{fo}, Su_g, Su_f, We_f, We_{fo}, We_g, and We_{go} predicting test data points from individual databases of (a) Ong [48], (b) Ducoulombier [45], (c) Copetti et al. [52], (d) Sempértegui-Tapia & Ribatski [74], (e) Sempértegui-Tapia & Ribatski [73], (f) Consolini [38], (g) Agostini et al. [37], and (h) Grauso at el. [64].

Table 6
Dimensionless parametric variation for the consolidated database and data from some selected databases.

	Consolidated database Data points: 16593			Sempértegui-Tapia & Ribatski (2017) and Xu et al. (2016) Data points: 910			Grauso et al. (2013) Data points: 575			Anwar et al. (2015) Data points: 256			Wang et al. (2014) Data points: 127		
Parameter	Mean	Min.	Max.	Mean	Min.	Max.	Mean	Min.	Max.	Mean	Min.	Max.	Mean	Min.	Max.
Bd	7.05	0.00	98.61	1.78	0.35	5.93	41.17	37.10	44.20	4.47	4.45	4.83	15.48	13.56	17.75
Bo	7.32E−04	3.10E−05	2.17E−02	4.63E-04	1.19E−04	1.09E−03	1.98E−04	5.27E−05	7.58E−04	1.07E-03	2.78E−04	1.94E−03	1.04E−03	3.83E−04	1.93E−03
Co	0.84	0.00	240.05	0.34	0.00	6.42	0.24	0.01	5.62	0.86	0.00	13.29	0.14	0.00	0.64
Fr_f	15.88	0.00	434.51	8.00	0.00	76.29	0.47	0.00	3.04	3.97	0.00	13.41	0.09	0.00	0.41
Fr_{fo}	32.46	0.02	439.11	25.17	1.15	104.55	1.32	0.24	3.09	7.16	0.54	13.54	0.31	0.21	0.55
Fr_g	18957	0	2899757	8283	3	144268	2328	1	14803	736	0	9553	1422	15	8381
Fr_{go}	2220191	27	3.3E+08	25801	1589	165345	7891	1611	20863	5108	395	9868	4895	921	17514
Pe_f	8813	7	181846	4638	44	16517	16340	798	51306	8788	86	17752	4393	71	9727
Pe_g	18393	3	485744	15909	491	49374	73375	1556	202143	12554	300	59034	26738	5102	51772
Pr_f	3.69	0.91	8.92	3.34	3.23	3.49	3.94	3.63	4.34	3.38	3.33	3.39	3.16	2.98	3.33
Pr_g	0.94	0.67	6.70	0.89	0.86	0.92	0.85	0.83	0.86	0.93	0.93	0.95	0.80	0.79	0.82
Re_f	2445.88	1.95	55245.35	1389.04	13.22	4966.69	4155.99	195.22	12526.84	2599.40	25.30	5243.74	1397.16	23.01	3003.04
Re_{fo}	3819.89	27.15	55270.00	2573.33	959.91	5536.82	8127.50	3555.83	12618.96	3705.09	1054.02	5270.09	2920.15	2104.74	3465.23
Re_g	19250	3	359795	17912	534	55623	86176	1813	239906	13539	324	63734	33342	6342	65722
Re_{go}	59179	624	410952	38853	14526	83696	176185	76253	274167	45255	12955	64777	64607	58445	95008
Su_f	444463	29502	3136613	268459	126598	523231	1306194	1147092	1414625	444096	441318	444281	1770801	1535952	2014012
Su_g	2875745	35116	1.4E+07	2003255	938859	3899121	8230288	6160430	1.0E+07	2483134	2432171	2486531	8901015	6761349	1.1E+07
We_f	27.06	0.00	3139.79	10.15	0.00	85.95	19.51	0.03	124.13	18.51	0.00	61.89	1.40	0.00	5.55
We_{fo}	54.17	0.01	3142.59	28.74	4.03	106.82	55.09	9.97	125.96	33.31	2.50	62.51	4.85	2.88	7.47
We_g	231.06	0.00	20918.88	235.47	0.16	1426.48	1235.92	0.46	6727.71	126.46	0.04	1633.63	159.69	4.15	638.83
We_{go}	1777.61	1.37	32696.92	878.87	123.29	3336.55	4176.26	810.82	10353.55	887.93	67.50	1687.53	515.81	306.64	1335.01

3.3. Predicting unseen data with ANN

ANN models have poor performance for predicting dependent variables which are outside the convex hull of the training data as it is not generalized for the unseen data. [95,96]. Till now, we have used the complete consolidated database which includes the 50 sources to generate a training dataset, develop the ANN model, and predict the corresponding test dataset. It was seen that the ANN model developed was observed to do a reasonably good job with *MAE* of 14.3%. As we are working with a new predicting technique, for the soft computing algorithm to be acceptable for predictions, it should be able to learn from known information and use that knowledge to predict unknown information including completely unknown datasets. Therefore, it is also important to understand how the model will perform if we used it to predict databases outside its training set. In this section, we test various ANN models by excluding one or two databases and predicting the corresponding saturated flow boiling heat transfer coefficients.

Fig. 10(a) shows the ANN model predictions when Sempértegui-Tapia & Ribatski [73] and Xu et al. [72] were excluded from the training database which consisted of the 48 remaining sources [28-68,71-77]. We can see that when predicting the whole databases of Sempértegui-Tapia & Ribatski [73] and Xu et al. [72], the ANN model gives a low *MAE* of 18.7%, and the percentage data predicted within ±30% is 86.5% and percentage data predicted within ±50% is 94.8%. Specifically, it can be seen from Table 1 that R134a is the most common working fluid being investigated by various researchers and has been tested over a variety of operating and geometric conditions. Therefore, the remaining database should haves enough information for the parametric range under investigation by Sempértegui-Tapia & Ribatski [73] and Xu et al. [72], thus giving a low *MAE*. These two databases combined, included 910 datapoints, and Table 6 shows parametric variation of this database. Fig.11(a) and 11(b) shows the experimental data and corresponding predictions of local heat transfer coefficient vs. vapor quality for some selected data from Sempértegui-Tapia & Ribatski [73] and Xu et al. [72], respectively. For Sempértegui-Tapia & Ribatski [73] with heat fluxes ranging from 1.5 W/cm^2 to 4.5 W/cm^2 as shown in Fig.11(a), not only are the local values of heat transfer coefficients predicted with good accuracy but also the trend in heat transfer variation with vapor quality are captured by the model. It clearly captures the initial almost negligible change in heat transfer for the lower ranges of vapor quality before a steeper increase, something expected in a convective dominant boiling heat transfer regime. For Xu et al. [72] with heat fluxes ranging from 2.7 W/cm^2 to 3.5 W/cm^2 as shown in Fig. 11(b), we can see the model capturing the trends to a certain extent, but overpredicting the heat transfer coefficient in the high quality region.

Next, we test ANN models by excluding one of the databases and predicting the corresponding saturated flow boiling heat transfer coefficients for that excluded dataset. After excluding data from Charnay et al. [67] in ANN model development, the corresponding ANN model could predict this database with *MAE* of 15.2% as shown in Fig. 10(b). Similarly, after excluding data from Anwar et al. [69] in ANN model development, the corresponding ANN model could predict this database with *MAE* of 20.3% as shown in Fig. 10(c). For Charnay et al. [67] and Anwar et al. [69], the overall *MAE* is low, but there are some outliers. One main reason for reasonably good model predictions is that similar to R134a data by Sempértegui-Tapia & Ribatski [73] and Xu et al. [72], the remaining test database has enough information for the parametric range under investigating including a number of datapoints for the working fluids, R245fa and R1234yf. Table 6 shows parametric variation of these two databases. Fig.11(c) and 11(d) shows the experimental data and corresponding predictions of local heat transfer coefficient vs. vapor quality for some selected data from Charnay

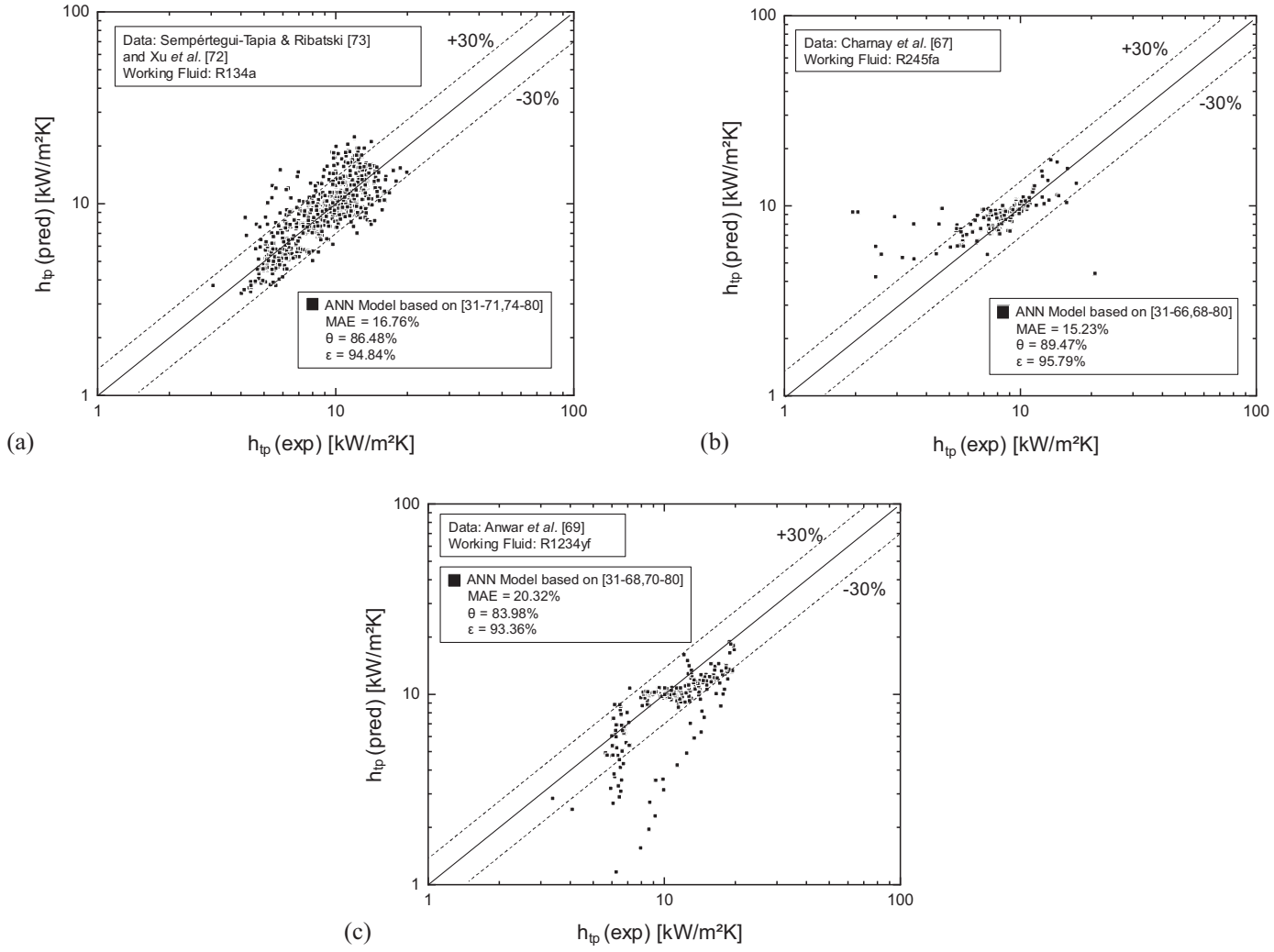

Fig. 10. ANN model with hidden layers (75,70,60,50,30,20,10) and input parameters Bd, Bo, Co, Fr_f, Fr_{fo}, Fr_g, Fr_{go}, Pr_f, Pr_g, Re_g, Re_f, Re_{go}, Re_{fo}, Su_g, Su_f, We_f, We_{fo}, We_g, and We_{go} predicting data points from excluded datasets of (a) Sempértegui-Tapia & Ribatski [73] and Xu et al. [72], (b) Charnay et al. [67], and (c) Anwar et al. [69].

et al. [67] and Anwar et al. [69], respectively. For both cases, the local values and variations in heat transfer coefficient are captured reasonably well. Some variations in numbers and trends are seen in the low quality as well as in some cases the high quality regions of the plot. As these are the regions where heat transfer changes show larger changes over small vapor quality variations as depicted in Fig. 2, higher chances of underpredicting or overpredicting exist here.

Next, we test ANN models by excluding one of the databases that is based on a fluid not used in the training dataset. This database is by Wang et al. [68] and here the working fluid is propane. The results as seen in Fig. 12(a) show that the ANN model did an extremely poor job with *MAE* of 197.3%. This clearly shows that for situations such as this where the working fluid has no past data for training, the model might not be able to capture the heat transfer variation accurately. When we look at the overall parametric variation of the dimensionless input parameters used to train the ANN model as shown in Table 6, we can see that like other datasets tested in Fig. 10, the parametric variation in Wang et al. [68] is within the maximum and minimum ranges for the consolidated databases, showing that the consolidated database includes to some extent the information needed for predicting data by Wang et al. [68]. Data from Wang et al. [68] does not change the minimum and maximum values for consolidated database parameters in Table 6. However, if we look closely, some specific parametric differences can be observed between the database by Wang et al. [68] and the consolidated database. Specific to the data for Wang et al. [68], the dimensionless numbers, Fr_f, Fr_{fo}, We_f and We_{fo} vary significantly from the mean data of the consolidated database. These variations do not directly show the reason for poor model predictions, but point out to the fact that the current database might include less information about the range of parameters needed to accurately predict Wang et al. [68]. On the other hand the databases by Sempértegui-Tapia & Ribatski [73], Xu et al. [72], Charnay et al. [67] and Anwar et al. [69], show values that are closer to the mean in comparison to Wang et al. [68]. To check the contribution of these parameters, we modified the ANN model by excluding these 4 parameters. ANN model with input parameters, *Bd, Bo, Co,* Fr_g, Fr_{go}, Pr_g, Pr_f, Re_g, Re_{go}, Re_f, Re_{fo}, Su_g, Su_f, We_g and We_{go}, and hidden layers (75,70,60,50,30,20,10) when used to predict excluded data from Wang et al. [68] gave *MAE* of 39.6% to predict this dataset, an improvement but now the data is underpredicted as seen in Fig. 12(b). Hence, even with the improvement, the remaining parameters cannot capture the trends accurately and might not be directly excluded from the model. In addition, it should be noted that in the original predicted data plotted in Fig. 7, when Wang et al. [68] was part of the training dataset, it gave an *MAE* of 22.5% for the test data from its database. This

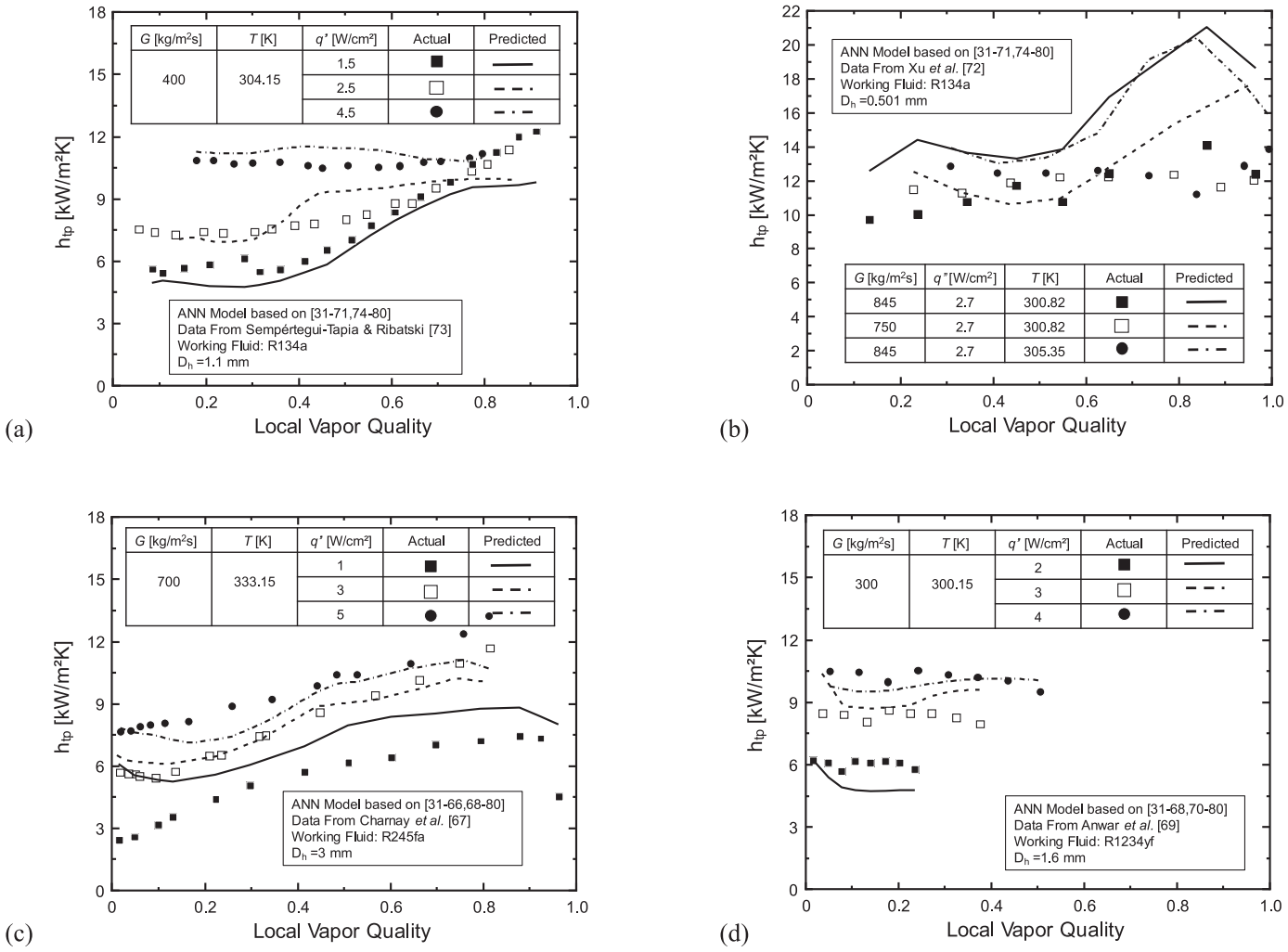

Fig. 11. ANN model with hidden layers (75,70,60,50,30,20,10) and input parameters Bd, Bo, Co, Fr_f, Fr_{fo}, Fr_g, Fr_{go}, Pr_f, Pr_g, Re_g, Re_f, Re_{go}, Re_{fo}, Su_g, Su_f, We_f, We_{fo}, We_g, and We_{go} predicting local heat transfer coefficients vs. vapor quality of excluded data for (a) Sempértegui-Tapia & Ribatski [73], (b) and Xu et al. [72], (c) Charnay et al. [67], and (d) Anwar et al. [69].

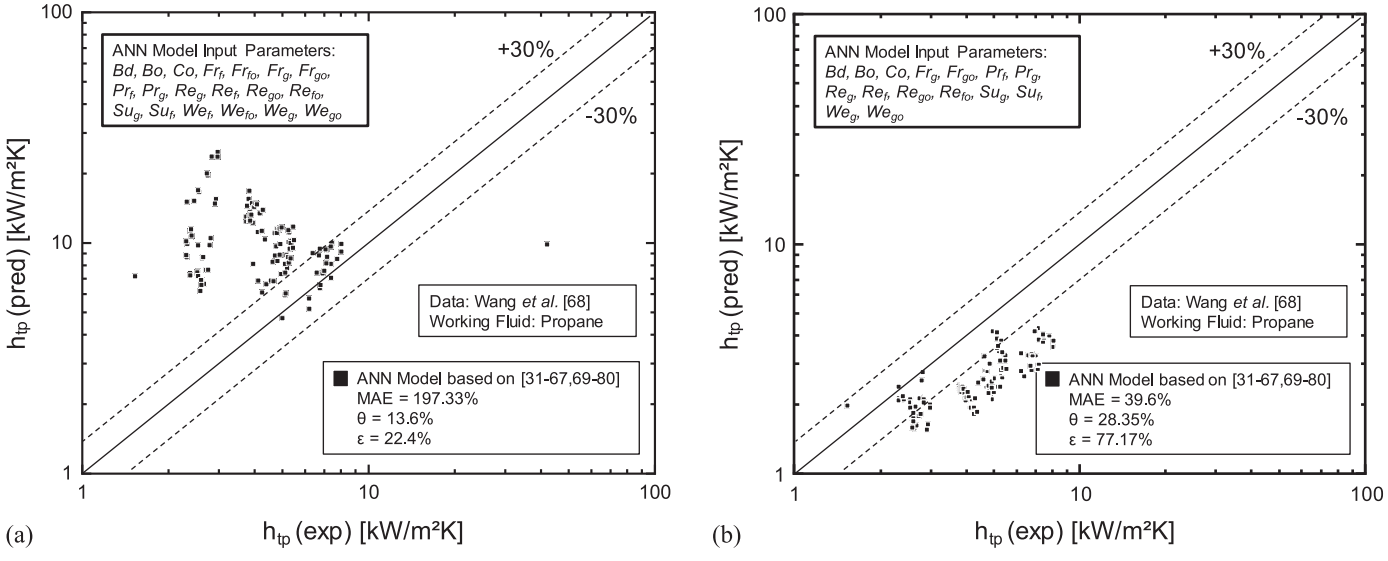

Fig. 12. ANN model with hidden layers (75,70,60,50,30,20,10) predicting excluded data of Wang et al. [68] with (a) input parameters Bd, Bo, Co, Fr_f, Fr_{fo}, Fr_g, Fr_{go}, Pr_f, Pr_g, Re_g, Re_f, Re_{go}, Re_{fo}, Su_g, Su_f, We_f, We_{fo}, We_g, and We_{go} and (b) input parameters Bd, Bo, Co, Fr_g, Fr_{go}, Pr_f, Pr_g, Re_g, Re_f, Re_{go}, Re_{fo}, Su_g, Su_f, We_g, and We_{go}.

is higher than the *MAE* of the consolidated data that was 14.3%; however, the result is not as bad as when we excluded the dataset from the model development as seen in Fig. 12(a).

The use of a universal ANN model utilizing a consolidated database as that developed in the current study becomes a useful tool when it can predict test cases for geometric and operating parameters which might not be within its parametric range. However, ANN models rely strongly on available data and its correlations to the output parameter, in this case the heat transfer coefficient, and more datapoints will certainly improve the predicting capability. This is seen in the results in Fig. 10(a)–(c) where without providing any data from those databases, the model was able to predict the heat transfer coefficients reasonably well. When less data is available for the model development, like that observed in Fig. 12(a), we should be careful in directly utilizing the ANN model as a predicting tool. Over time, however, it is possible that we amass more data for such working fluids and include more parametric variations that the ANN model will learn to predict data for such databases.

4. Conclusions

In this study, a new method for prediction heat transfer coefficient for saturated flow boiling in mini/micro channels is proposed. A universal consolidated database is used to develop a machine learning based predictive modeling approach for predicting the data. Key findings from this study are as follows:

A consolidated database of 16953 data points for flow boiling heat transfer in mini/micro-channels is amassed from 50 sources. This included 16 working fluid, reduced pressures of 0.0046–0.77, hydraulic diameters of 0.15 mm–6.5 mm, mass velocities of $19 < G < 1608$ kg/m^{2}s, liquid-only Reynolds numbers of 27 – 55270 and flow qualities of 0–1. The database included circular and rectangular channels, single-channel and multi-channels, and uniform and non-uniform heating in vertical and horizontal orientations with respect to gravity

The consolidated database is split into train and test data. An optimization is conducted and the final model architecture consists of dimensionless input parameters: *Bd, Bo, Co,* Fr_g, Fr_{go}, Fr_f, Fr_{fo}, Pr_g, Pr_f, Re_g, Re_{go}, Re_f, Re_{fo}, Su_g, Su_f, We_g, We_{go}, We_f, and We_{fo} and hidden layers (75,70,60,50,30,20,10). This ANN model shows very good accuracy in predicting the test data with an *MAE* of 14.3%, and the percentage data predicted within ±30% and ±50% is 92.0% and is 97.4%, respectively.

The ANN model predicting capability is compared with universal correlations for saturated flow boiling heat transfer. The ANN model is superior to the highly reliable universal correlation by Kim and Mudawar [3] at predicting the test data, even predicting individual databases with high accuracy.

The ANN model is modified by excluding certain databases from the training datasets and utilized to predict the excluded databases. The ANN model did an extremely good job in predicting some databases which included working fluids and parameters that are in the training dataset, and poorly when a working fluid data was excluded from training dataset. By showing that the ANN model could predict test cases from databases unseen by the training model, the use of a universal ANN model can become an extremely useful tool when it comes to predicting heat transfer coefficients for saturated flow boiling in mini/micro channels.

Author declaration

We confirm that the manuscript has been read and approved by all named authors and that there are no other persons who satisfied the criteria for authorship but are not listed. We further confirm that the order of authors listed in the manuscript has been approved by all of us.

We confirm that we have given due consideration to the protection of intellectual property associated with this work and that there are no impediments to publication, including the timing of publication, with respect to intellectual property. In so doing we confirm that we have followed the regulations of our institutions concerning intellectual property.

We understand that the Corresponding Author is the sole contact for the Editorial process (including Editorial Manager and direct communications with the office). He/she is responsible for communicating with the other authors about progress, submissions of revisions and final approval of proofs. We confirm that we have provided a current, correct email address which is accessible by the Corresponding Author and which has been configured to accept email from chirag.kharangate@case.edu

CRediT authorship contribution statement

Yue Qiu: Validation, Investigation, Writing - original draft. **Deepak Garg:** Conceptualization, Methodology, Software, Writing - original draft. Liwei **Zhou:** Formal analysis, Investigation, Data curation. **Chirag R. Kharangate:** Conceptualization, Methodology, Supervision, Writing - original draft, Writing - review & editing. **Sung-Min Kim :** Data curation, Writing - original draft. **Issam Mudawar:** Methodology, Writing - review & editing.

Declaration of Competing Interest

We wish to confirm that there are no known conflicts of interest associated with this publication and there has been no significant financial support for this work that could have influenced its outcome.

Supplementary materials

Supplementary material associated with this article can be found, in the online version, at doi:10.1016/j.ijheatmasstransfer.2019.119211.

CRediT authorship contribution statement

Yue Qiu: Validation, Investigation, Writing - original draft. **Deepak Garg:** Conceptualization, Methodology, Software, Writing - original draft. **Liwei Zhou:** Formal analysis, Investigation, Data curation. **Chirag R. Kharangate:** Conceptualization, Methodology, Supervision, Writing - original draft, Writing - review & editing. **Sung-Min Kim:** Data curation, Writing - original draft. **Issam Mudawar:** Methodology, Writing - review & editing.

References

[1] I. Mudawar, Recent advances in high-flux, two-phase thermal management, J. Therm. Sci. Eng. Appl. (2013) 5, doi:10.1115/1.4023599.
[2] I. Mudawar, Two-phase microchannel heat sinks: theory, applications, and limitations, J. Electron. Packag. 133 (2011) 41002–41031, doi:10.1115/1.4005300.
[3] S.M. Kim, I. Mudawar, Universal approach to predicting saturated flow boiling heat transfer in mini/micro-channels – Part II. Two-phase heat transfer coefficient, Int. J. Heat Mass Transf. 64 (2013) 1239–1256, doi:10.1016/j.ijheatmasstransfer.2013.04.014.
[4] G.M. Lazarek, S.H. Black, Evaporative heat transfer, pressure drop and critical heat flux in a small vertical tube with R-113, Int. J. Heat Mass Transf. 25 (1982) 945–960, doi:10.1016/0017-9310(82)90070-9.
[5] M.M. Shah, Chart correlation for saturated boiling heat transfer: equations and further study., in: ASHRAE Trans., ASHRAE, 1982, pp. 185–196.
[6] S.M. Kim, I. Mudawar, Theoretical model for local heat transfer coefficient for annular flow boiling in circular mini/micro-channels, Int. J. Heat Mass Transf. 73 (2014) 731–742, doi:10.1016/j.ijheatmasstransfer.2014.02.055.
[7] M. Magnini, B. Pulvirenti, J.R. Thome, Numerical investigation of hydrodynamics and heat transfer of elongated bubbles during flow boiling in a microchannel, Int. J. Heat Mass Transf. 59 (2013) 451–471, doi:10.1016/j.ijheatmasstransfer.2012.12.010.

[8] T. KUNUGI, Direct numerical simulation of pool and forced convective flow boiling phenomena, Heat Transf 3 (2002) (2002) 497–502.
[9] K.F. GUNGOR, Simplified general correlation for saturrated flow boiling and comparison of correlation with data, Chem. Eng. Res. Dev. 65 (1987) 148.
[10] S.G. Kandlikar, A general correlation for saturated two-phase flow boiling heat transfer inside horizontal and vertical tubes, J. Heat Transf. 112 (1990) 219–228, doi:10.1115/1.2910348.
[11] Z. Liu, R.H.S. Winterton, A general correlation for saturated and subcooled flow boiling in tubes and annuli, based on a nucleate pool boiling equation, Int. J. Heat Mass Transf. 34 (1991) 2759–2766, doi:10.1016/0017-9310(91)90234-6.
[12] S.S. Bertsch, E.A. Groll, S.V. Garimella, A composite heat transfer correlation for saturated flow boiling in small channels, Int. J. Heat Mass Transf. 52 (2009) 2110–2118, doi:10.1016/J.IJHEATMASSTRANSFER.2008.10.022.
[13] X. Fang, Q. Wu, Y. Yuan, A general correlation for saturated flow boiling heat transfer in channels of various sizes and flow directions, Int. J. Heat Mass Transf. 107 (2017) 972–981, doi:10.1016/J.IJHEATMASSTRANSFER.2016.10.125.
[14] D.D. Massie, Optimization of a building's cooling plant for operating cost and energy use, Int. J. Therm. Sci. 41 (2002) 1121–1129, doi:10.1016/S1290-0729(02)01398-4.
[15] J. Yang, H. Rivard, R. Zmeureanu, On-line building energy prediction using adaptive artificial neural networks, Energy Build 37 (2005) 1250–1259, doi:10.1016/J.ENBUILD.2005.02.005.
[16] A. Abbassi, L. Bahar, Application of neural network for the modeling and control of evaporative condenser cooling load, Appl. Therm. Eng. 25 (2005) 3176–3186, doi:10.1016/J.APPLTHERMALENG.2005.04.006.
[17] S. Lecoeuche, S. Lalot, B. Desmet, Modelling a non-stationary single tube heat exchanger using multiple coupled local neural networks, Int. Commun. Heat Mass Transf. 32 (2005) 913–922, doi:10.1016/J.ICHEATMASSTRANSFER.2004.08.029.
[18] G. Dıáz, M. Sen, K.. Yang, R.L. McClain, Dynamic prediction and control of heat exchangers using artificial neural networks, Int. J. Heat Mass Transf. 44 (2001) 1671–1679, doi:10.1016/S0017-9310(00)00228-3.
[19] N. Bar, T.K. Bandyopadhyay, M.N. Biswas, S.K. Das, Prediction of pressure drop using artificial neural network for non-Newtonian liquid flow through piping components„ J. Pet. Sci. Eng. 71 (2010) 187–194, doi:10.1016/J.PETROL.2010.02.001.
[20] G. Díaz, M. Sen, K.T. Yang, R.L. McClain, Simulation of heat exchanger performance by artificial neural networks, HVAC&R Res 5 (1999) 195–208, doi:10.1080/10789669.1999.10391233.
[21] A. Pacheco-Vega, M. Sen, R.L. McClain, Analysis of fin-tube evaporator performance with limited experimental data using artificial neural networks, ASME-PUBLICATIONS-HTD 366 (2000) 95–102.
[22] J. Thibault, B.P.A. Grandjean, A neural network methodology for heat transfer data analysis, Int. J. Heat Mass Transf. 34 (1991) 2063–2070, doi:10.1016/0017-9310(91)90217-3.
[23] K. Jambunathan, S.L. Hartle, S. Ashforth-Frost, V.N. Fontama, Evaluating convective heat transfer coefficients using neural networks, Int. J. Heat Mass Transf. 39 (1996) 2329–2332, doi:10.1016/0017-9310(95)00332-0.
[24] A. Mazzola, Integrating artificial neural networks and empirical correlations for the prediction of water-subcooled critical heat flux, Rev. Générale Therm. 36 (1997) 799–806, doi:10.1016/S0035-3159(97)87750-1.
[25] P. Naphon, T. Arisariyawong, Heat transfer analysis using artificial neural networks of the spirally fluted tubes, J. Res. Appl. Mech. Eng. 4 (2016) 135–147.
[26] P. Naphon, T. Arisariyawong, T. Nualboonrueng, Artificial neural network analysis on the heat transfer and friction factor of the double tube with spring insert, Int. J. Appl. Eng. Res. 11 (2016) 3542–3549.
[27] A.M. Ghahdarijani, F. Hormozi, A.H. Asl, Convective heat transfer and pressure drop study on nanofluids in double-walled reactor by developing an optimal multilayer perceptron artificial neural network, Int. Commun. Heat Mass Transf. 84 (2017) 11–19, doi:10.1016/J.ICHEATMASSTRANSFER.2017.03.014.
[28] M. Mehrabi, M. Sharifpur, J.P. Meyer, Modelling and multi-objective optimisation of the convective heat transfer characteristics and pressure drop of low concentration TiO2-water nanofluids in the turbulent flow regime, Int. J. Heat Mass Transf. 67 (2013) 646–653, doi:10.1016/j.ijheatmasstransfer.2013.08.013.
[29] P. Naphon, S. Wiriyasart, T. Arisariyawong, Artificial neural network analysis the pulsating Nusselt number and friction factor of TiO2/water nanofluids in the spirally coiled tube with magnetic field, Int. J. Heat Mass Transf. 118 (2018) 1152–1159, doi:10.1016/j.ijheatmasstransfer.2017.11.091.
[30] P. Naphon, S. Wiriyasart, T. Arisariyawong, L. Nakharintr, ANN, numerical and experimental analysis on the jet impingement nanofluids flow and heat transfer characteristics in the micro-channel heat sink, Int. J. Heat Mass Transf. 131 (2019) 329–340, doi:10.1016/j.ijheatmasstransfer.2018.11.073.
[31] M.W. Wambsganss, D.M. France, J.A. Jendrzejczyk, T.N. Tran, Boiling heat transfer in a horizontal small-diameter tube, J. Heat Transfer 115 (1993) 963–972.
[32] T.N. Tran, Pressure drop and heat transfer study of two-phase flow in small channels [dissertation], TX: Texas Tech University, Lubbock, 1999.
[33] S. Saitoh, H. Daiguji, E. Hihara, Effect of tube diameter on boiling heat transfer of R-134a in horizontal small-diameter tubes, Int. J. Heat Mass Transf. 48 (2005) 4973–4984, doi:10.1016/J.IJHEATMASSTRANSFER.2005.03.035.
[34] R. Yun, Y. Kim, M.S. Kim, Convective boiling heat transfer characteristics of CO2 in microchannels, Int. J. Heat Mass Transf. 48 (2005) 235–242, doi:10.1016/J.IJHEATMASSTRANSFER.2004.08.019.
[35] R. Muwanga, I. Hassan, A flow boiling heat transfer investigation of FC-72 in a microtube using liquid crystal thermography, J. Heat Transf. 129 (2006) 977–987, doi:10.1115/1.2728905.
[36] X. Zhao, P.K. Bansal, Flow boiling heat transfer characteristics of CO2 at low temperatures, Int. J. Refrig. 30 (2007) 937–945, doi:10.1016/J.IJREFRIG.2007.02.010.
[37] B. Agostini, J.R. Thome, M. Fabbri, B. Michel, D. Calmi, U. Kloter, High heat flux flow boiling in silicon multi-microchannels – Part I: Heat transfer characteristics of refrigerant R236fa, Int. J. Heat Mass Transf. 51 (2008) 5400–5414, doi:10.1016/J.IJHEATMASSTRANSFER.2008.03.006.
[38] L. Consolini, Convective boiling heat transfer in a single micro-channel, EPFL PP – Lausanne, n.d. 10.5075/epfl-thesis-4024.
[39] S.S. Bertsch, E.A. Groll, S.V. Garimella, Effects of heat flux, mass flux, vapor quality, and saturation temperature on flow boiling heat transfer in microchannels, Int. J. Multiph. Flow. 35 (2009) 142–154, doi:10.1016/J.IJMULTIPHASEFLOW.2008.10.004.
[40] S. In, S. Jeong, Flow boiling heat transfer characteristics of R123 and R134a in a micro-channel, Int. J. Multiph. Flow. 35 (2009) 987–1000, doi:10.1016/J.IJMULTIPHASEFLOW.2009.07.003.
[41] R. Mastrullo, A.W. Mauro, A. Rosato, G.P. Vanoli, Carbon dioxide local heat transfer coefficients during flow boiling in a horizontal circular smooth tube, Int. J. Heat Mass Transf. 52 (2009) 4184–4194, doi:10.1016/J.IJHEATMASSTRANSFER.2009.04.004.
[42] H. Ohta, K. Inoue, M. Ando, K. Watanabe, Experimental investigation on observed scattering in heat transfer characteristics for flow boiling in a small diameter tube, Heat Transf. Eng. 30 (2009) 19–27, doi:10.1080/01457630802290080.
[43] C.-C. Wang, C.-S. Chiang, J.-G. Yu, An experimental study of in-tube evaporation of R-22 inside a 6.5-mm smooth tube, Int. J. Heat Fluid Flow. 19 (1998) 259–269, doi:10.1016/S0142-727X(98)00006-X.
[44] L. Wang, M. Chen, M. Groll, Flow Boiling Heat Transfer Characteristics of R134a in a Horizontal Mini Tube, J. Chem. Eng. Data. 54 (2009) 2638–2645, doi:10.1021/je900140w.
[45] M. Ducoulombier, Ebullition convective du dioxyde de carbone-étude expérimentale en micro-canal [dissertation], France: University of Insa Lyon, Villeurbanne, 2010.
[46] M. Hamdar, A. Zoughaib, D. Clodic, Flow boiling heat transfer and pressure drop of pure HFC-152a in a horizontal mini-channel, Int. J. Refrig. 33 (2010) 566–577, doi:10.1016/J.IJREFRIG.2009.12.006.
[47] C. Martin Callizo, Flow boiling heat transfer in single vertical channels of small diameter [dissertation], KTH Royal Institute of Technology, Stockholm, Sweden, 2010.
[48] C.L. Ong, Macro-to-microchannel transition in two-phase flow and evaporation, in: Proceedings of the EPFL, 2010.
[49] C.B. Tibiriçá, G. Ribatski, Flow boiling heat transfer of R134a and R245fa in a 2.3 mm tube, Int. J. Heat Mass Transf. 53 (2010) 2459–2468, doi:10.1016/J.IJHEATMASSTRANSFER.2010.01.038.
[50] R. Ali, B. Palm, M.H. Maqbool, Flow boiling heat transfer characteristics of a minichannel up to dryout condition, J. Heat Transfer. (2011) 133, doi:10.1115/1.4003669.
[51] K.H. Bang, K.K. Kim, S.K. Lee, B.W. Lee, Pressure effect on flow boiling heat transfer of water in minichannels, Int. J. Therm. Sci. 50 (2011) 280–286, doi:10.1016/J.IJTHERMALSCI.2010.03.011.
[52] J.B. Copetti, M.H. Macagnan, F. Zinani, N.L.F. Kunsler, Flow boiling heat transfer and pressure drop of R-134a in a mini tube: an experimental investigation, Exp. Therm. Fluid Sci. 35 (2011) 636–644, doi:10.1016/J.EXPTHERMFLUSCI.2010.12.013.
[53] M.M. Mahmoud, T.G. Karayiannis, D.B.R. Kenning, Surface effects in flow boiling of R134a in microtubes, Int. J. Heat Mass Transf. 54 (2011) 3334–3346, doi:10.1016/J.IJHEATMASSTRANSFER.2011.03.052.
[54] Y.-Y. Yan, T.-F. Lin, Evaporation heat transfer and pressure drop of refrigerant R-134a in a small pipe, Int. J. Heat Mass Transf. 41 (1998) 4183–4194, doi:10.1016/S0017-9310(98)00127-6.
[55] H.-K. Oh, C.-H. Son, Flow boiling heat transfer and pressure drop characteristics of CO2 in horizontal tube of 4.57-mm inner diameter, Appl. Therm. Eng. 31 (2011) 163–172, doi:10.1016/J.APPLTHERMALENG.2010.08.026.
[56] H.-K. Oh, C.-H. Son, Evaporation flow pattern and heat transfer of R-22 and R-134a in small diameter tubes, Heat Mass Transf. 47 (2011) 703–717, doi:10.1007/s00231-011-0761-4.
[57] J. Wu, T. Koettig, C. Franke, D. Helmer, T. Eisel, F. Haug, J. Bremer, Investigation of heat transfer and pressure drop of CO_2 two-phase flow in a horizontal minichannel, Int. J. Heat Mass Transf. 54 (2011) 2154–2162, doi:10.1016/J.IJHEATMASSTRANSFER.2010.12.009.
[58] E. Costa-Patry, J. Olivier, J. Thome, Heat transfer charcacteristics in a copper micro-evaporator and flow pattern-based prediction method for flow boiling in microchannels, Front. Heat Mass Transf. 3 (2012).
[59] T.G. Karayiannis, M.M. Mahmoud, D.B.R. Kenning, A study of discrepancies in flow boiling results in small to microdiameter metallic tubes, Exp. Therm. Fluid Sci. 36 (2012) 126–142, doi:10.1016/J.EXPTHERMFLUSCI.2011.09.005.
[60] M. Li, C. Dang, E. Hihara, Flow boiling heat transfer of HFO1234yf and R32 refrigerant mixtures in a smooth horizontal tube: Part I. Experimental investigation, Int. J. Heat Mass Transf. 55 (2012) 3437–3446, doi:10.1016/J.IJHEATMASSTRANSFER.2012.03.002.
[61] C.B. Tibiriçá, G. Ribatski, J.R. Thome, Flow boiling characteristics for R1234ze (E) in 1.0 and 2.2mm circular channels, J. Heat Transf. 134 (2012) 20906.
[62] K. Balasubramanian, M. Jagirdar, P.S. Lee, C.J. Teo, S.K. Chou, Experimental investigation of flow boiling heat transfer and instabilities in straight microchannels, Int. J. Heat Mass Transf. 66 (2013) 655–671, doi:10.1016/J.IJHEATMASSTRANSFER.2013.07.050.

[63] D. Del Col, S. Bortolin, D. Torresin, A. Cavallini, Flow boiling of R1234yf in a 1 mm diameter channel, Int. J. Refrig. 36 (2013) 353–362, doi:10.1016/J.IJREFRIG.2012.10.026.
[64] S. Grauso, R. Mastrullo, A.W. Mauro, J.R. Thome, G.P. Vanoli, Flow pattern map, heat transfer and pressure drops during evaporation of R-1234ze(E) and R134a in a horizontal, circular smooth tube: Experiments and assessment of predictive methods, Int. J. Refrig. 36 (2013) 478–491, doi:10.1016/J.IJREFRIG.2012.07.016.
[65] Z.Y. Bao, D.F. Fletcher, B.S. Haynes, Flow boiling heat transfer of Freon R11 and HCFC123 in narrow passages, Int. J. Heat Mass Transf. 43 (2000) 3347–3358, doi:10.1016/S0017-9310(99)00379-8.
[66] F. Vakili-Farahani, B. Agostini, J.R. Thome, Experimental study on flow boiling heat transfer of multiport tubes with R245fa and R1234ze(E), Int. J. Refrig. 36 (2013) 335–352, doi:10.1016/J.IJREFRIG.2012.12.007.
[67] R. Charnay, R. Revellin, J. Bonjour, Flow boiling characteristics of R-245fa in a minichannel at medium saturation temperatures, Exp. Therm. Fluid Sci. 59 (2014) 184–194, doi:10.1016/J.EXPTHERMFLUSCI.2014.01.011.
[68] S. Wang, M.Q. Gong, G.F. Chen, Z.H. Sun, J.F. Wu, Two-phase heat transfer and pressure drop of propane during saturated flow boiling inside a horizontal tube, Int. J. Refrig. 41 (2014) 200–209, doi:10.1016/J.IJREFRIG.2013.03.019.
[69] Z. Anwar, B. Palm, R. Khodabandeh, Flow boiling heat transfer, pressure drop and dryout characteristics of R1234yf: experimental results and predictions, Exp. Therm. Fluid Sci. 66 (2015) 137–149, doi:10.1016/J.EXPTHERMFLUSCI.2015.03.021.
[70] R. Charnay, R. Revellin, J. Bonjour, Flow boiling heat transfer in minichannels at high saturation temperatures: Part I – Experimental investigation and analysis of the heat transfer mechanisms, Int. J. Heat Mass Transf. 87 (2015) 636–652, doi:10.1016/J.IJHEATMASSTRANSFER.2015.03.081.
[71] B. Markal, O. Aydin, M. Avci, An experimental investigation of saturated flow boiling heat transfer and pressure drop in square microchannels, Int. J. Refrig. 65 (2016) 1–11, doi:10.1016/J.IJREFRIG.2015.12.013.
[72] Y. Xu, X. Fang, G. Li, D. Li, Y. Yuan, An experimental study of flow boiling heat transfer of R134a and evaluation of existing correlations, Int. J. Heat Mass Transf. 92 (2016) 1143–1157, doi:10.1016/J.IJHEATMASSTRANSFER.2015.09.044.
[73] D.F. Sempértegui-Tapia, G. Ribatski, The effect of the cross-sectional geometry on saturated flow boiling heat transfer in horizontal micro-scale channels, Exp. Therm. Fluid Sci. 89 (2017) 98–109, doi:10.1016/J.EXPTHERMFLUSCI.2017.08.001.
[74] D.F. Sempértegui-Tapia, G. Ribatski, Flow boiling heat transfer of R134a and low GWP refrigerants in a horizontal micro-scale channel, Int. J. Heat Mass Transf. 108 (2017) 2417–2432, doi:10.1016/J.IJHEATMASSTRANSFER.2017.01.036.
[75] E.M. Fayyadh, M.M. Mahmoud, K. Sefiane, T.G. Karayiannis, Flow boiling heat transfer of R134a in multi microchannels, Int. J. Heat Mass Transf. 110 (2017) 422–436, doi:10.1016/J.IJHEATMASSTRANSFER.2017.03.057.
[76] W. Qu, I. Mudawar, Flow boiling heat transfer in two-phase micro-channel heat sinks – -I. Experimental investigation and assessment of correlation methods, Int. J. Heat Mass Transf. 46 (2003) 2755–2771, doi:10.1016/S0017-9310(03)00041-3.
[77] B. Sumith, F. Kaminaga, K. Matsumura, Saturated flow boiling of water in a vertical small diameter tube, Exp. Therm. Fluid Sci. 27 (2003) 789–801, doi:10.1016/S0894-1777(02)00317-5.
[78] R. Yun, Y. Kim, M. Soo Kim, Y. Choi, Boiling heat transfer and dryout phenomenon of CO_2 in a horizontal smooth tube, Int. J. Heat Mass Transf. 46 (2003) 2353–2361, doi:10.1016/S0017-9310(02)00540-9.
[79] X. Huo, L. Chen, Y.S. Tian, T.G. Karayiannis, Flow boiling and flow regimes in small diameter tubes, Appl. Therm. Eng. 24 (2004) 1225–1239, doi:10.1016/J.APPLTHERMALENG.2003.11.027.
[80] J. Lee, I. Mudawar, Two-phase flow in high-heat-flux micro-channel heat sink for refrigeration cooling applications: Part II – heat transfer characteristics, Int. J. Heat Mass Transf. 48 (2005) 941–955, doi:10.1016/J.IJHEATMASSTRANSFER.2004.09.019.
[81] W.S. McCulloch, W. Pitts, A logical calculus of the ideas immanent in nervous activity, Bull. Math. Biophys. 5 (1943) 115–133, doi:10.1007/BF02478259.
[82] G.M. Maggiora, D.W. Elrod, R.G. Trenary, Computational neural networks as model-free mapping devices, J. Chem. Inf. Comput. Sci. 32 (1992) 732–741.
[83] D. Svozil, V. Kvasnička, J. Pospíchal, Introduction to multi-layer feed-forward neural networks, in: Chemometrics and Intelligent Laboratory Systems, Elsevier, 1997, pp. 43–62, doi:10.1016/S0169-7439(97)00061-0.
[84] A. Krizhevsky, I. Sutskever, G.E. Hinton, ImageNet classification with deep convolutional neural networks, in: F. Pereira, C.J.C. Burges, L. Bottou, K.Q. Weinberger (Eds.), Advances in Neural Information Processing Systems, 25, Associates, Inc., Curran, 2012, pp. 1097–1105.
[85] C.M. Bishop, Neural Networks for Pattern Recognition, Oxford university press, 1995.
[86] H. Rumelhart, G.E. Hinton, Williams, 1986."Back Propag. Train. Algorithm", Dev. MIT (1995).
[87] B.J. Wythoff, Backpropagation neural networks: A tutorial, Chemom. Intell. Lab. Syst. 18 (1993) 115–155, doi:10.1016/0169-7439(93)80052-J.
[88] A. Prieto, B. Prieto, E.M. Ortigosa, E. Ros, F. Pelayo, J. Ortega, I. Rojas, Neural networks: An overview of early research, current frameworks and new challenges, Neurocomputing 214 (2016) 242–268, doi:10.1016/J.NEUCOM.2016.06.014.
[89] M. Lehtokangas, J. Saarinen, K. Kaski, P. Huuhtanen, Initializing weights of a multilayer perceptron network by using the orthogonal least squares algorithm, Neural Comput. 7 (1995) 982–999, doi:10.1162/neco.1995.7.5.982.
[90] D.P. Kingma, J. Ba, in: Adam: a method for stochastic optimization, 3rd International Conference for Learning Representations, 2015 San Diego, CA.
[91] J. Brownlee, in: Machine Learning Mastery with Python, Mach. Learn. Mastery Pty Ltd., 2016, pp. 100–120.
[92] S. Haykin, Neural Networks: a Comprehensive Foundation, Prentice Hall PTR, 1994.
[93] G. James, D. Witten, T. Hastie, R. Tibshirani, An Introduction to Statistical Learning, Springer, 2013.
[94] S.-M. Kim, I. Mudawar, Universal approach to predicting saturated flow boiling heat transfer in mini/micro-channels – Part I. Dryout incipience quality, Int. J. Heat Mass Transf. 64 (2013) 1226–1238, doi:10.1016/J.IJHEATMASSTRANSFER.2013.04.016.
[95] P. Courrieu, Three algorithms for estimating the domain of validity of feedforward neural networks, Neural Netw. 7 (1994) 169–174, doi:10.1016/0893-6080(94)90065-5.
[96] A. Pacheco-Vega, M. Sen, K.T. Yang, R.L. McClain, Neural network analysis of fin-tube refrigerating heat exchanger with limited experimental data, Int. J. Heat Mass Transf. 44 (2001) 763–770, doi:10.1016/S0017-9310(00)00139-3.